Angewandte Chemie
Eine Zeitschrift der Gesellschaft Deutscher Chemiker

Supporting Information

Generation and Stabilization of a Dinickel Catalyst in a Metal-Organic Framework for Selective Hydrogenation Reactions

*Q.-Y. Guo, Z. Wang, X. Feng, Y. Fan, W. Lin**

Table of Contents

1. Materials and Methods

1.1 Chemicals and Solvents

All starting materials were purchased from Sigma-Aldrich and Fisher (USA) unless otherwise noted and used without further purification. All solvents used were dry and oxygen-free. All of the reactions and manipulations were carried out under N_2 with the use of standard inert atmosphere and Schlenk technique unless otherwise indicated. Substituted diphenylacetylene substrates were synthesized by palladium-catalyzed Sonogashira coupling following literature report.[1]

1.2 Characterizations

Transmission electron microscopy (TEM) was carried out on a TECNAI Spirit microscope.

Powder X-ray diffraction (PXRD) data were collected on SAXSLAB's GANESHA using transmission mode.

N_2 sorption measurements at 77 K were carried out on a Micromeritics 3FLEX instrument.

Inductively coupled plasma-mass spectrometry (ICP-MS) data was obtained with an Agilent 7700x ICP-MS and analyzed using ICP-MS Mass Hunter version B01.03. Samples were diluted in a 2% HNO_3 matrix and analyzed with a ^{159}Tb internal standard against a 12-point standard curve over the range from 0.1 ppb to 500 ppb. The correlation was > 0.9997 for all analyses of interest. Data collection was performed in Spectrum Mode with five replicates per sample and 100 sweeps per replicate.

X-ray photoelectron spectroscopy (XPS) data was collected using an AXIS Nova spectrometer (Kratos Analytical) with monochromatic Al Kα X-ray source; Al anode was powered at 10 mA and 15 kV, and the instrument work function was calibrated to give an Au $4f_{7/2}$ metallic gold binding energy (BE) of 83.95 eV. Instrument base pressure was ca. 1×10^{-9} Torr. The analysis area size was 0.3 × 0.7 mm^2. For calibration purposes, the binding energies were referenced to the C 1s peak at 284.8 eV. Survey spectra were collected with a step size of 1 eV and 160 eV pass energy.

Gas chromatography (GC) analysis was performed on a Shimadzu GC-2010 Plus gas chromatograph equipped with a flame ionization detector (FID). Column: SH-Rxi-5Sil MS column, 30.0 m in length, 0.25 mm in diameter, 0.25 μm in thickness. GC conditions: Injection temperature, 220 °C; Column temperature program, 30 °C hold for 5 min, followed by a ramp of 5 °C/min to 60 °C then a ramp of 10 °C/min to 300 °C; Column flow, 1.21 mL/min.

Nuclear magnetic resonance (NMR). ^1H and ^{13}C NMR spectra were recorded on a Bruker DRX at 400 and 101 MHz, respectively, referenced to the resonances resulting from the solvents. ^1H NMR Spectra were reported as follows: chemical shift (δ ppm), multiplicity (s = singlet, d = doublet, t = triplet, q = quartet, m = multiplet), coupling constants (Hz), integration and assignment.

Thermogravimetric analysis (TGA) was performed in air using a Shimazu TGA-50 equipped with a platinum pan and heated at a rate of 1.5 °C per min.

Electron Paramagnetic Resonance (EPR) spectroscopy was performed with a Bruker Elexsys 500 X-band EPR spectrometer. The temperature of the samples was held at 15K using an Oxford Systems continuous-flow He Cryostat coupled with a 10K He stinger from Bruker.

Fourier transformed infrared spectroscopy (FTIR) was performed using a Thermo NEXUS 670 Near-, Far-, and Mid-FTIR with attenuated total reflectance (ATR) accessory (for powder samples).

Energy dispersive spectrometry (EDS) was performed on a Carl Zeiss Merlin scaning electron miscroscopy (SEM) with the detectors of In-Lens, EsB, AsB, & SE2.

X-ray absorption (XAS) data was collected at Beamline 10-BM, Advanced Photon Source (APS), Argonne National Laboratory. Spectra were collected at the K-edge of Ni (8333 eV) in transmission mode. The X-ray beam was monochromatized by a Si (111) monochromator and detuned by 50% to reduce the contribution of higher-order harmonics below the level of noise. A metallic foil standard was used as a reference for energy calibration and was measured simultaneously with experimental samples. Samples were ground and mixed with polyethylene glycol (PEG) and packed in a Teflon wafer. XAS data was processed using the Athena and Artemis programs of the IFEFFIT package based on FEFF 6.1-2. Prior to merging. Fit of the EXAFS region was performed using the Artemis program of the IFEFFIT package.

2. Synthesis and Characterization of MOF-253, MOF-$NiBr_2$ and MOF-NiH

2.1 Synthesis and characterization of MOF-253

2.1.1 Synthesis of MOF-253

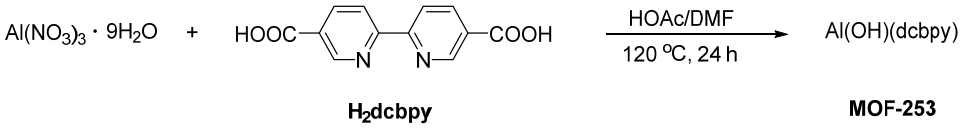

Figure S1. Synthesis of MOF-253.

MOF-253 was synthesized following a modified procedure based on literature report.[2] $Al(NO_3)_3{\cdot}9H_2O$ (235 mg, 0.625 mmol), 2, 2'-bipyridine-5, 5'-dicarboxylic acid (H_2dcbpy, 153 mg, 0.625 mmol), acetic acid (859 μL, 15.0 mmol) and N,N'-dimethylformamide (DMF) were mixed in a Schlenk flask. The resulting mixture was sonicated for 5 min, and stirred at 120 °C for 24 h. The resulting white powder was collected by centrifugation and sequentially washed with DMF three times, THF three times, and benzene three times. The resulting solid was freeze-dried in benzene to afford white powder as the desired product. Acetic acid was omitted in the synthesis of MOF-253 for porosity test.[2]

2.1.2 TEM of MOF-253

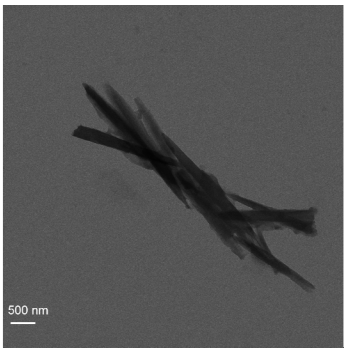

Figure S2. TEM image of MOF-253. A needle-like morphology of microcrystal was revealed.

2.2 Synthesis and characterization of MOF-$NiBr_2$

2.2.1 Synthesis of MOF-$NiBr_2$

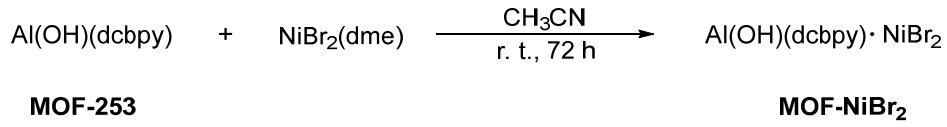

Figure S3. Synthesis of MOF-$NiBr_2$.

In a N_2-filled glovebox, nickel bromide ethylene glycol dimethyl ether complex ($NiBr_2$(dme), 200 mg, 0.65 mmol) was weighed out in a 100 mL glass bottle equipped with a plastic cap, 80 mL of anhydrous acetonitrile (CH_3CN) was then added and stirred at room temperature for 24 h to allow the complete dissolution of the nickel salt. MOF-253 (40 mg, 0.13 mmol) was then added into the solution. The resulting mixture was stirred at room temperature in a glovebox for 72 h. The light green solid was centrifuged and washed with anhydrous CH_3CN three times. The resulting solid was then heated at 100 °C under vacuum for 24 h to afford a yellow solid as the desired product.

2.2.2 Thermogravimetric analysis (TGA) of MOF-$NiBr_2$

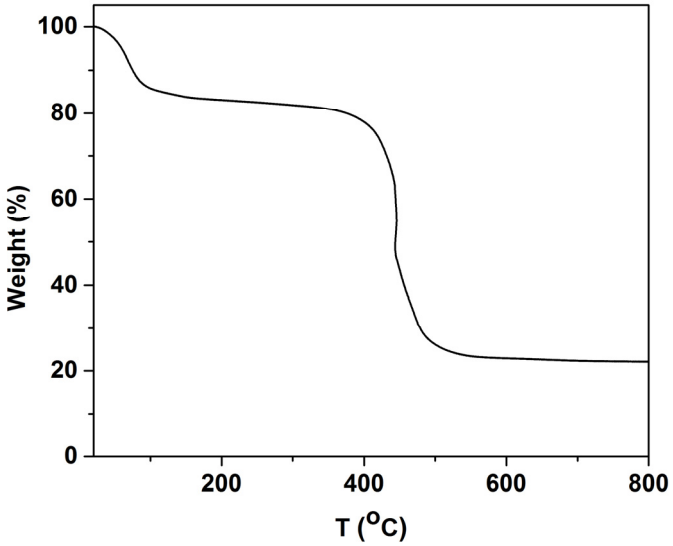

Figure S4. TGA curve of MOF-$NiBr_2$. The first weight loss of 17.5% from 25 °C to 130 °C corresponds to the removal of adsorbed solvents in the MOF pores. The second weight loss of 60.1% from 370 °C to 570 °C corresponds to the decomposition of the MOF to metal oxides.

2.2.3 X-ray photoelectron spectroscopy (XPS) of MOF-$NiBr_2$

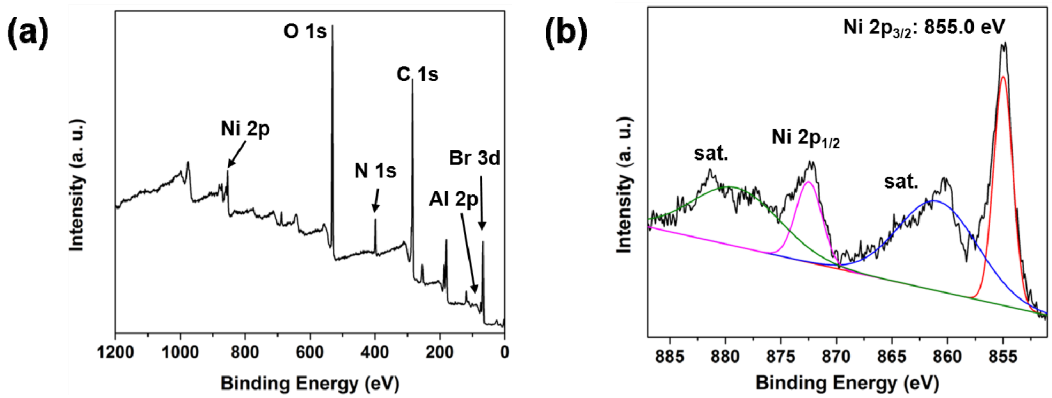

Figure S5. XPS spectra of (a) the survey scan and (b) Ni 2p of MOF-$NiBr_2$. The XPS survey spectrum indicated the existence of Al, C, O, N, Ni and Br in MOF-$NiBr_2$. The high-resolution spectra of Ni 2p showed a Ni $2p_{3/2}$ peak position at 855.0 eV, which indicated a +2 oxidation state of nickel.[3]

2.3 Synthesis and characterization of MOF-NiH

2.3.1 Synthesis of MOF-NiH

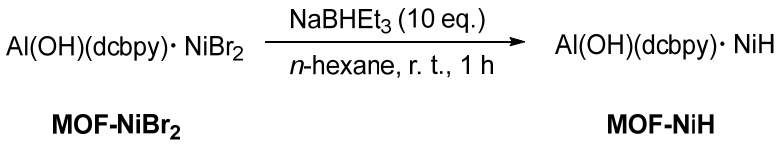

Figure S6. Synthesis of MOF-NiH.

In a N_2-filled glovebox, MOF-$NiBr_2$ (2.5 mg, 5 μmol) was charged to a 1.5 mL centrifuge tube and dispersed in 1.0 mL of *n*-hexane. $NaBHEt_3$ (50 μL, 50 μmol, 1.0 M solution in THF) was then added dropwise to the suspension. The color of the MOF changed immediately from yellow to dark green with vigorous evolution of H_2 gas. The resulting suspension was kept at room temperature for 1 h to ensure complete conversion. The dark green solid was centrifuged and washed with *n*-hexane three times.

2.3.2 Extended X-ray adsorption fine structure (EXAFS) studies of MOF-NiH

MOF-NiH X-ray absorption data was collected and processed through identical protocol at Beamline 10-BM-A, B at the advanced photon source (APS) at Argonne National Laboratory. Fitting result are shown in **Figure 3d**. Fitting parameters are listed below.

Table S1. Summary of EXAFS fitting parameters of MOF-NiH

MOF-NiH		**Fitting Range**	k: 3.0-14.1 $Å^{-1}$ R: 1-3.0 Å
Independent Points	13.8	**Variables**	6
Reduced chi-square	990	**R-factor**	0.02
ΔE (eV)	-8.05	**amp**	2.80
R(Ni-H) (2)	1.60 ± 0.09 Å	**σ^2 (Ni-H)**	0.002

R(Ni-N) (2)	1.90 ± 0.09 Å	**σ^2 (Ni-N)**	0.004
R(Ni-Ni) (1)	2.31 ± 0.20 Å	**σ^2 (Ni-Ni)**	0.013
R(Ni-C_{30}) (2)	2.72 ± 0.02 Å	**σ^2 (Ni-C_{30})**	0.003
R(Ni-C_5) (1)	2.90 ± 0.04 Å	**σ^2 (Ni-C_5)**	0.002
R(Ni-C_{17}) (1)	2.94 ± 0.07 Å	**σ^2 (Ni-C_{17})**	0.002

2.3.3 X-ray photoelectron spectroscopy (XPS) of MOF-NiH

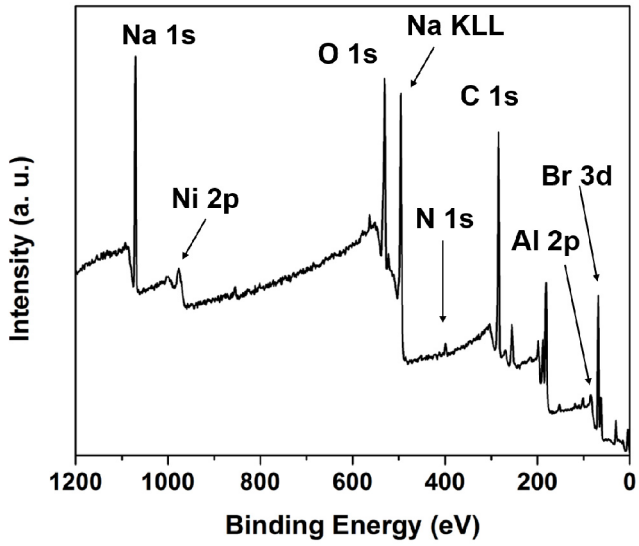

Figure S7. XPS survey spectrum of MOF-NiH. The XPS survey spectrum of MOF-NiH showed the existence of Ni, Al, C, O, N in the sample. The signal of Na and Br comes from the byproduct NaBr formed during $NaBHEt_3$ treatment, which cannot be removed by *n*-hexane washing due to the poor solubility of NaBr in *n*-hexane.

2.3.4 Fourier-transformed infrared spectroscopy (FTIR) of MOF-NiH

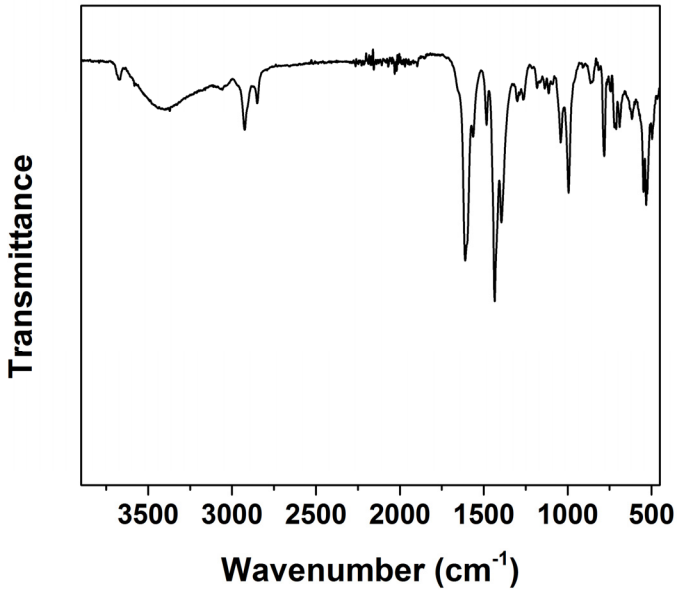

Figure S8. FTIR spectrum of MOF-NiH.

2.3.5 Thermogravitric analysis (TGA) of MOF-NiH

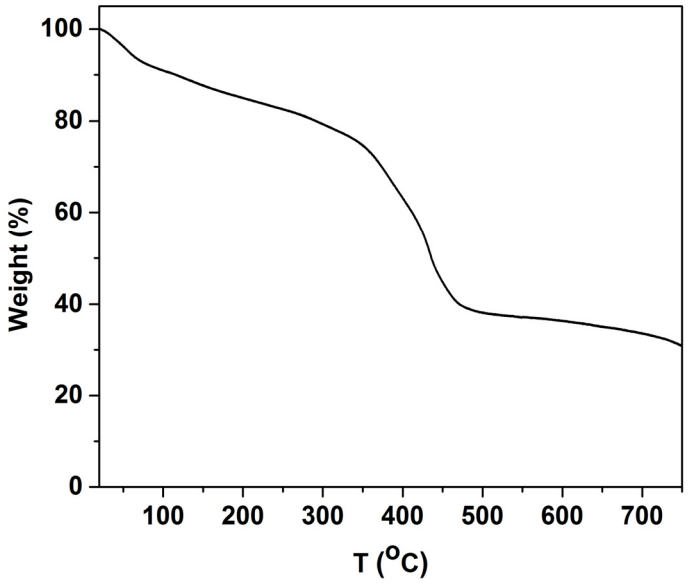

Figure S9. TGA curve of MOF-NiH. The first weight loss of 24.2 % from 25 °C to 340 °C corresponds to the removal of adsorbed solvents in the MOF pores. The second weight loss of 36.8 % from 340 °C to 480 °C corresponds to the decomposition of the MOF to metal oxides. NaBr formed during $NaBHEt_3$ treatment remained in the final pyrolyzed solid, which results in higher residual weight compared with MOF-$NiBr_2$.

2.3.6 Energy dispersive spectrometry (EDS) mapping of MOF-NiH

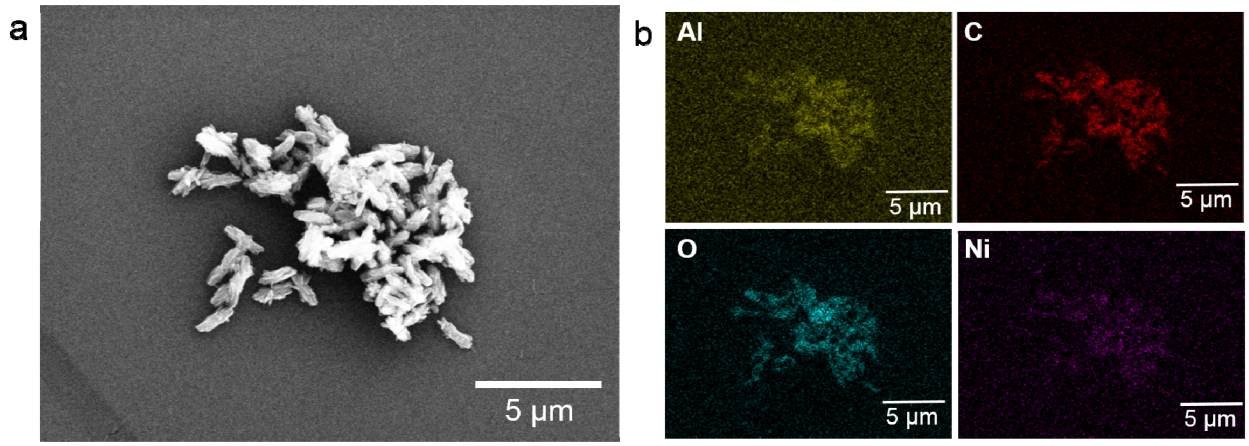

Figure S10. (a) SEM image and (b) corresponding EDS mapping results of MOF-NiH. The existence of Al, C, O, Ni in MOF microcrystals was confirmed.

2.3.7 Nitrogen adorption experiment of MOF-NiH

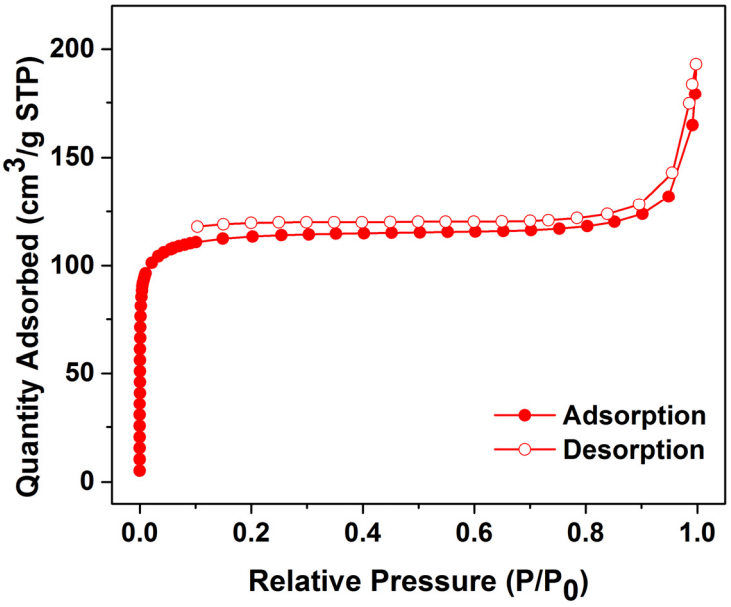

Figure S11. N_2 adsorption isotherm of MOF-NiH at 77 K. The BET surface area was calculated as 364 m^2/g.

2.3.8 Quantification of H_2 produced from protonation of MOF-NiH

The quantification of H_2 produced from protonation of MOF-NiH was performed following a previously reported procedure.[4-5] In a Schlenk tube, MOF-NiH (10 μmol of Ni) was dispersed in 1 mL benzene, formic acid (1.8 μL, 100 μmol) was added through the rubber stopper by a syringe. After reacting at room temperature for 1 h, the head space was analyzed by gas chromatography (GC) to quantify the amount of generated H_2. Consistent results were obtained in three runs. The amount of H_2 generated was calculated as 14.7 ± 2.4 μmol (expected 15 μmol).

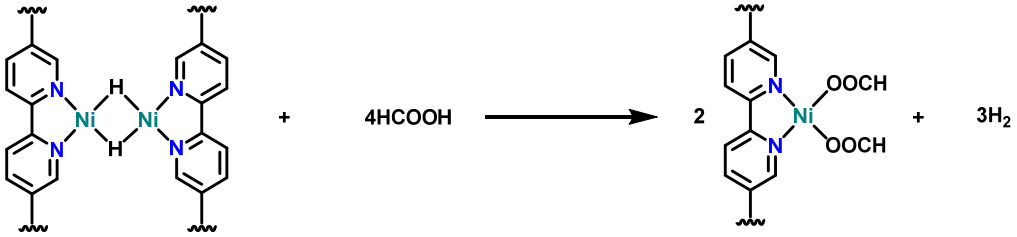

Figure S12. Hydrogen quantification during protonation of MOF-NiH.

2.4 Synthesis and characterization of mononuclear catalyst MOF-NiH_1

2.4.1 Synthesis of MOF-0.12$NiBr_2$

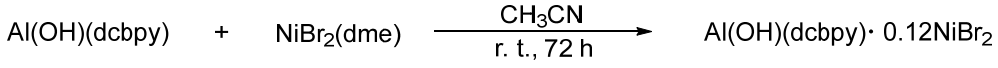

MOF-253 **MOF-0.12$NiBr_2$**

Figure S13. Synthesis of MOF-0.12$NiBr_2$.

In a N_2-filled glovebox, $NiBr_2$(dme) (4.0 mg, 0.013 mmol) was weighed out in a 20 mL glass vial, 10 mL acetonitrile was then added and stirred at room temperature for 24 h to allow the dissolution of the nickel source. MOF-253 (30 mg, 0.11 mmol) was then added

into the solution. The resulting mixture was stirred at room temperature in the glovebox for 72 h. The light green solid was centrifuged and washed with anhydrous CH_3CN three times. The resulting solid was then heated at 100 °C under vacuum for 24 h to afford light yellow solid as the desired product. The loading of Ni was determined by ICP-MS as 0.12, so the formula was written as MOF-0.12$NiBr_2$.

2.4.2 Synthesis of MOF-NiH_1

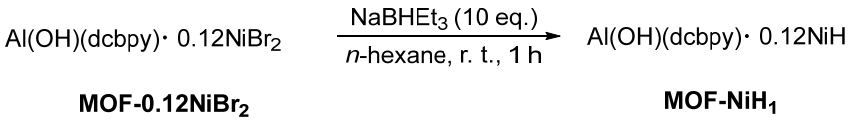

Figure S14. Synthesis of MOF-NiH_1.

In a N_2-filled glovebox, MOF-0.12$NiBr_2$ (13.0 mg, 5 μmol Ni) was charged to a 1.5 mL centrifuge tube and dispersed in 1.0 mL of *n*-hexane. $NaBHEt_3$ (50 μL, 50 μmol, 1.0 M solution in THF) was then added dropwise to the suspension. The color of MOF changed immediately from yellow to dark green with vigorous evolution of H_2 gas. The resulting suspension was kept at room temperature for 1 h to ensure the complete conversion. The dark green solid was centrifuged and washed with *n*-hexane three times.

2.4.3 Powder X-ray diffraction (PXRD) of MOF-NiH_1

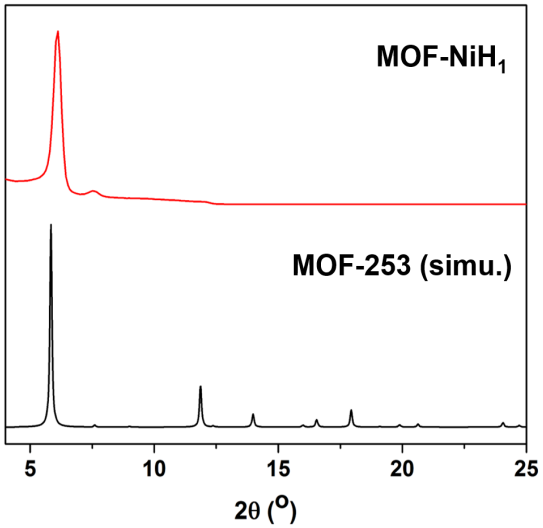

Figure S15. The sililarity of PXRD patterns of MOF-NiH_1 (red) to the simulated pattern of MOF-253 (black).

2.4.4 Nitrogen adsortion experiment of MOF-NiH_1

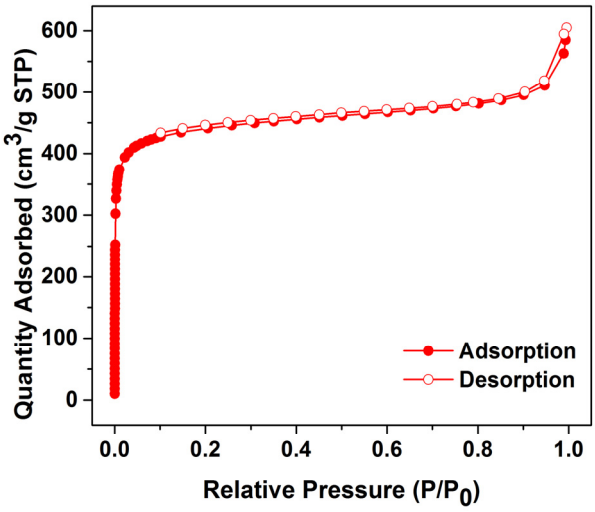

Figure S16. N_2 adsorption isotherm of mononuclear catalyst MOF-NiH_1 at 77 K. The BET surface area was calculated as 1406 m^2/g.

3. Catalytic Reactions and Characterization of Products

General procedure for semi-hydrogenation of internal alkynes. In a N_2-filled glovebox, MOF-NiH (2.5 μmol) was dispersed in *n*-hexane (1 mL; for substrates **1f-1j**, cyclohexane was used instead) and transferred into a Parr reactor. Alkyne substrates (0.25 mmol) and additional *n*-hexane (2 mL; for substrates **1f-1j**, cyclohexane was used instead) were then added subsequently. The Parr reactor was then sealed under nitrogen, and charged with H_2 to 5 bar. After stirring at 50 °C for 72 h, the pressure was released and the MOF catalyst was removed from the reaction mixture via filtration. The solvent was removed by reduced pressure to afford the crude product, which was further analyzed by GC-MS or purified by column chromatography to afford semi-hydrogenation products **2a-2j**. The reaction condition for each substrate was optimized to give the optimal result. In GC-MS analysis, the ratios of (*Z*)-stilbene derivatives to overhydrogenated products were determined by ^1H NMR due to the partial overlap of GC peaks.

General procedure for hydrogenation of α, β-unsaturated aldehydes and ketones. In a N_2-filled glovebox, MOF-NiH (2.5 μmol) was dispersed in cyclohexane (1 mL) and transferred into a Parr reactor. α, β-unsaturated aldehyde/ketones (0.50 mmol) and additional cyclohexane (2 mL) were then added subsequently. The Parr reactor was then sealed under nitrogen, and charged with H_2 to 10 bar. After stirring at 90 °C for 48 h (reaction times and temperatures vary for different substrates), the pressure was released and the MOF catalyst was removed from the reaction mixture via filtration. The solvent was removed by reduced pressure to afford the crude product, which was further purified by column chromatography to afford hydrogenation products **6a-6f**. The reaction condition for each substrate was optimized to give the optimal result.

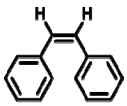

2a

Colorless oil, 80% yield. ^1H NMR (400 MHz, $CDCl_3$): δ 7.30-7.18 (m, 10H), 6.62 (s, 2H); ^{13}C NMR (101 MHz, $CDCl_3$): δ 137.26, 130.26, 128.99, 128.22, 127.10.

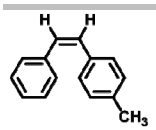

2b

Colorless oil, 74% yield. ^{1}H NMR (400 MHz, $CDCl_3$): δ 7.29-7.17 (m, 5H), 7.15 (d, *J* = 8.2Hz, 2H), 7.03 (d, *J* = 8.2Hz, 2H), 6.56 (s, 2H), 2.31 (s, 3H); ^{13}C NMR (101 MHz, $CDCl_3$): δ 137.50, 136.87, 134.26, 130.20, 129.55, 128.90, 128.84, 128.79, 128.19, 126.96, 21.25.

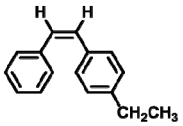

2c

Colorless oil, 86% yield. ^{1}H NMR (400 MHz, $CDCl_3$): δ 7.34-7.18 (m, 7H), 7.08 (d, *J* = 8.0Hz, 2H), 6.59 (s, 2H), 2.64 (q, *J* = 7.6Hz, 2H), 1.25 (t, *J* = 7.6Hz, 3H); ^{13}C NMR (101 MHz, $CDCl_3$): δ 143.24, 137.53, 134.49, 130.21, 129.54, 128.84, 128.67, 128.19, 127.67, 126.96, 28.59, 15.40.

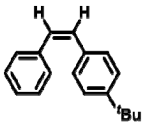

2d

Colorless oil, 70% yield. ^{1}H NMR (400 MHz, $CDCl_3$): δ 7.34-7.19 (m, 9H), 6.59 (s, 2H), 1.33 (s, 9H); ^{13}C NMR (101 MHz, $CDCl_3$): δ 150.17, 137.61, 134.19, 130.09, 129.57, 128.81, 128.58, 128.21, 126.96, 125.08, 34.56, 31.29.

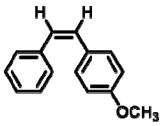

2e

Colorless oil, 87% yield. ^{1}H NMR (400 MHz, $CDCl_3$): δ 7.30-7.15 (m, 7H), 6.76 (d, *J* = 8.8Hz, 2H), 6.54 (d, *J* = 12.3Hz, 1H), 6.51 (s, *J* = 12.3Hz, 1H), 3.79 (s, 3H); ^{13}C NMR (101 MHz, $CDCl_3$): δ 158.71, 137.66, 130.19, 129.81, 129.70, 128.85, 128.83, 128.27, 126.94, 113.63, 55.23.

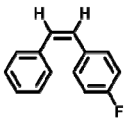

2f

Colorless oil, 62% yield. ^{1}H NMR (400 MHz, $CDCl_3$): δ 7.27-7.16 (m, 7H), 6.91 (t, *J* = 8.7 Hz, 2H), 6.60 (d, *J* = 12.2 Hz, 1H), 6.54 (d, *J* = 12.2 Hz, 1H); ^{13}C NMR (101 MHz, $CDCl_3$): δ 163.03, 160.58, 137.02, 133.19, 130.55, 130.24, 129.06, 128.81, 128.29, 127.18, 115.24, 115.03.

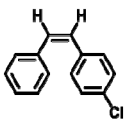

2g

Colorless oil, 89% yield. ^{1}H NMR (400 MHz, $CDCl_3$): δ 7.32-7.16 (m, 9H), 6.66 (d, *J* = 12.2 Hz, 1H), 6.56 (d, *J* = 12.2 Hz, 1H); ^{13}C NMR (101 MHz, $CDCl_3$): δ 136.87, 135.65, 132.75, 130.95, 130.22, 128.92, 128.81, 128.41, 128.34, 127.32.

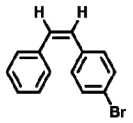

2h

Colorless oil, 89% yield. ^{1}H NMR (400 MHz, $CDCl_3$): δ 7.37 (d, *J* = 8.4 Hz, 2H), 7.27-7.16 (m, 5H), 7.14 (d, *J* = 8.3 Hz, 2H), 6.67 (d, *J* = 12.2 Hz, 1H), 6.54 (d, *J* = 12.2 Hz, 1H); ^{13}C NMR (101 MHz, $CDCl_3$): δ 136.86, 136.13, 131.39, 131.06, 130.56, 128.97, 128.82, 128.38, 127.38, 120.97.

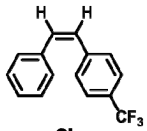

2j

Colorless oil, 73% yield. ^{1}H NMR (400 MHz, $CDCl_3$): δ 7.47 (d, *J* = 8.2 Hz, 2H), 7.33 (d, *J* = 8.3 Hz, 2H), 7.30-7.18 (m, 5H), 6.72 (d, *J* = 12.2 Hz, 1H), 6.60 (d, *J* = 12.2 Hz, 1H); ^{13}C NMR (101 MHz, $CDCl_3$): δ 140.92, 136.55, 132.33, 129.14, 128.82, 128.74, 128.43, 127.58, 125.54, 125.21, 125.17, 125.14, 125.10, 122.84.

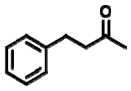

6b

Colorless oil. 96% yield. ^{1}H NMR (400 MHz, $CDCl_3$): δ 7.31-7.16 (m, 5H), 2.90 (t, *J* = 7.8 Hz, 2H), 2.76 (t, *J* = 7.8 Hz, 2H), 2.14 (s, 3H). ^{13}C NMR (101 MHz, $CDCl_3$): δ 207.96, 141.00, 128.51, 128.30, 126.12, 45.19, 30.08.

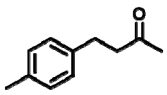

6c

Colorless oil, 75% yield. ^{1}H NMR (400 MHz, $CDCl_3$): δ 7.09 (d, *J* = 8.5 Hz, 2H), 7.07 (d, *J* = 8.5 Hz, 2H), 2.86 (t, *J* = 7.7 Hz, 2H), 2.74 (t, *J* = 7.7 Hz, 2H), 2.31 (s, 3H), 2.13 (s, 3H); ^{13}C NMR (101 MHz, $CDCl_3$): 208.12, 137.89, 135.59, 129.18, 128.17, 45.35, 30.08, 29.36, 21.00.

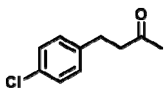

6d

Colorless oil, 82% yield. ^{1}H NMR (400 MHz, $CDCl_3$): δ 7.24 (d, *J* = 8.4 Hz, 2H), 7.11 (d, *J* = 8.4 Hz, 2H), 2.86 (t, *J* = 7.4 Hz, 2H), 2.74 (t, *J* = 7.4 Hz, 2H), 2.14 (s, 3H); ^{13}C NMR (101 MHz, $CDCl_3$): 207.46, 139.47, 131.85, 129.70, 128.57, 44.90, 30.10, 28.99.

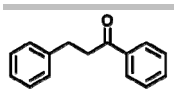

6e

White solid, 79% yield. ^{1}H NMR (400 MHz, $CDCl_3$): δ 7.96 (d, *J* = 7.2 Hz, 2H), 7.56 (t, *J* = 7.2 Hz, 1H), 7.45 (t, *J* = 7.2 Hz, 2H), 7.33-7.18 (m, 5H), 3.31 (t, *J* = 7.4 Hz, 2H), 3.07 (t, *J* = 7.4 Hz, 2H); ^{13}C NMR (101 MHz, $CDCl_3$): 199.22, 141.30, 136.87, 133.07, 128.61, 128.54, 128.43, 128.05, 126.14, 40.47, 30.15.

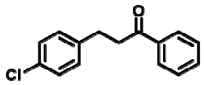

6f

White solid, 61% yield. ^{1}H NMR (400 MHz, $CDCl_3$): δ 7.95 (d, *J* = 7.2 Hz, 2H), 7.56 (t, *J* = 7.2 Hz, 1H), 7.46 (t, *J* = 7.2 Hz, 2H), 7.26 (d, *J* = 8.4 Hz, 2H), 7.19 (d, *J* = 8.4 Hz, 2H), 3.28 (t, *J* = 7.4 Hz, 2H), 3.04 (t, *J* = 7.4 Hz, 2H); ^{13}C NMR (101 MHz, $CDCl_3$): 198.82, 139.75, 136.76, 133.18, 131.87, 129.84, 128.65, 128.60, 128.02, 40.14, 29.39.

4. Control Experiments and Recycling Experiments

4.1 Control experiments

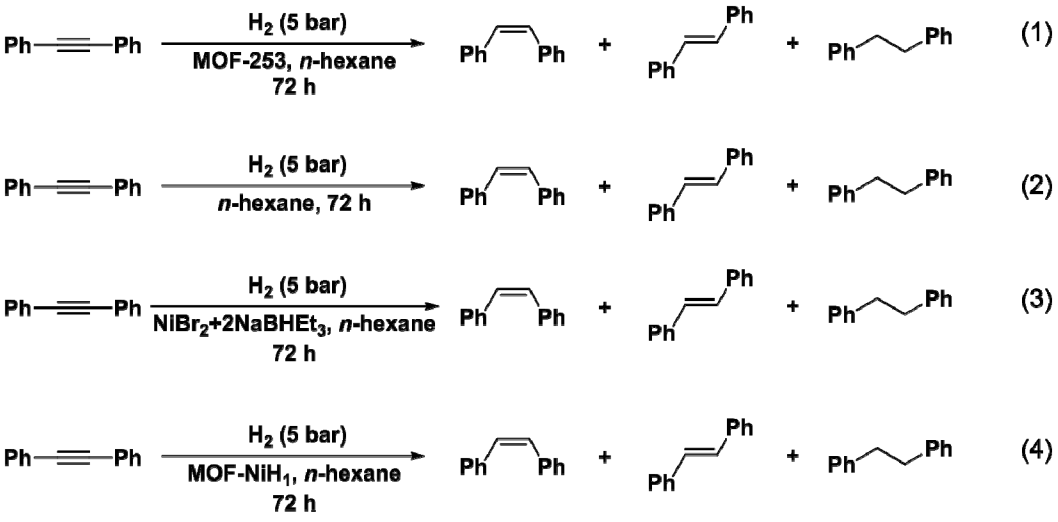

Figure S17. Control experiments.

Control reaction 1 using MOF-253 as catalyst. In a N_2-filled glovebox, MOF-253 (1.5 mg, 5 μmol) was dispersed in *n*-hexane (1 mL) and transferred into a Parr reactor. Dipheylacetylene (44.5 mg, 0.25 mmol) and additional *n*-hexane (2 mL) were then added subsequently. The Parr reactor was then sealed under nitrogen, and charged with H_2 to 5 bar. After stirring at 50 ºC for 72 h, the

pressure was released and the MOF catalyst was removed from the reaction mixture via filtration. The solvent was removed by reduced pressure to afford the crude product, which was further analyzed by GC-MS.

Control reaction 2 without a catalyst. In a N_2-filled glovebox, dipheylacetylene (44.5 mg, 0.25 mmol) and *n*-hexane (3 mL) were added subsequently into a Parr reactor. The Parr reactor was then sealed under nitrogen, and charged with H_2 to 5 bar. After stirring at 50 °C for 72 h, the pressure was released. The solvent was removed by reduced pressure to afford the crude product, which was further analyzed by crude ^{1}H NMR using CH_2Br_2 as internal standard.

Control reaction 3 using $NiBr_2$ and $NaBHEt_3$ as catalyst. In a N_2-filled glovebox, dipheylacetylene (44.5 mg, 0.25 mmol) and *n*-hexane (3 mL) was added subsequently into a Parr reactor. Then $NiBr_2$ (1.1 mg, 5 μmol) and $NaBHEt_3$ (10 μL, 10μmol, 1.0 M solution in THF) were added subsequently. The Parr reactor was then sealed under nitrogen, and charged with H_2 to 5 bar. After stirring at 50 °C for 72 h, the pressure was released and the catalyst was removed from the reaction mixture via filtration. The solvent was removed by reduced pressure to afford the crude product, which was further analyzed by crude ^{1}H NMR using CH_2Br_2 as internal standard.

Control reaction 4 using mononuclear catalyst MOF-NiH_1 as catalyst. In a N_2-filled glovebox, MOF-NiH_1 (13.0 mg, 5 μmol Ni) was dispersed in *n*-hexane (1 mL) and transferred into a Parr reactor. Dipheylacetylene (44.5 mg, 0.25 mmol) and additional *n*-hexane (2 mL) were then added subsequently. The Parr reactor was then sealed under nitrogen, and charged with H_2 to 5 bar. After stirring at 50 °C for 72 h, the pressure was released and the MOF catalyst was removed from the reaction mixture via filtration. The solvent was removed by reduced pressure to afford the crude product, which was further analyzed by crude ^{1}H NMR using CH_2Br_2 as internal standard.

4.2 Recycling experiments

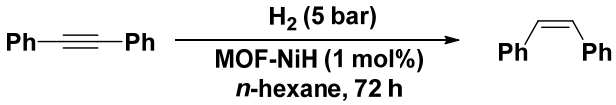

Figure S18. Recycle experiments.

In a N_2-filled glovebox, MOF-NiH (2.5 μmol) was dispersed in *n*-hexane (1 mL) and transferred into a Parr reactor. Diphenylacetylene (44.5 mg, 0.25 mmol) and additional *n*-hexane (2 mL) were then added subsequently. The Parr reactor was then sealed under nitrogen, and charged with H_2 to 5 bar. After stirring at 50 °C for 72 h, the pressure was released and the MOF catalyst was removed from the reaction mixture via centrifugation. The supernatant was transferred to a glass vial, and the MOF was washed by *n*-hexane 3 times for further use. The solvent of supernatant was removed by reduced pressure. The yield was then determined by ^{1}H NMR using CH_2Br_2 as internal standard. The recovered MOF catalyst was used for subsequent cycles of reactions. The reaction mixture of diphenylacetylene (44.5 mg, 0.25 mmol) and recovered MOF catalyst in 3 mL *n*-hexane was stirred at 50 °C for 72 h under 5 bar H_2 in each run.

Table S2. Yields of (*Z*)-stilbene in five consecutive runs of the recycling experiments.

Run	1	2	3	4	5
Yield (%)	76	80	74	63	60

4.3 Determination of metal leaching in the supernatant

In a N_2-filled glovebox, MOF-NiH (2.5 μmol) was dispersed in *n*-hexane (1 mL) and transferred into a Parr reactor. Diphenylacetylene (44.5 mg, 0.25 mmol) and additional *n*-hexane (2 mL) were then added subsequently. The Parr reactor was then sealed under nitrogen, and charged with H_2 to 5 bar. After stirring at 50 °C for 72 h, the pressure was released and the MOF catalyst was removed from the reaction mixture via centrifugation. The supernatant was transferred to a glass vial, and the solvent was removed by reduced pressure, then digested with a mixture of HF (15 μL), HCl (200 μL) and HNO_3 (200 μL) for 24 h. The resulting digested solution was further diluted to 10 mL and analyzed by ICP-MS.

4.4 Chracterizations of recycled catalyst

4.4.1 FTIR of recycled MOF-NiH

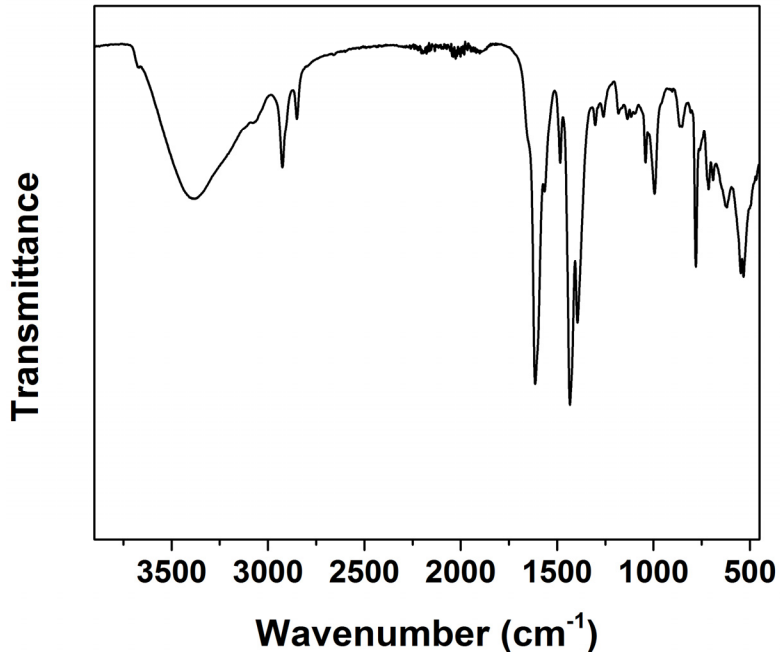

Figure S19. FTIR spectrum of the recycled MOF-NiH, which is almost identical with that of freshly prepared MOF-NiH catalyst.

4.4.2 XPS of recycled MOF-NiH

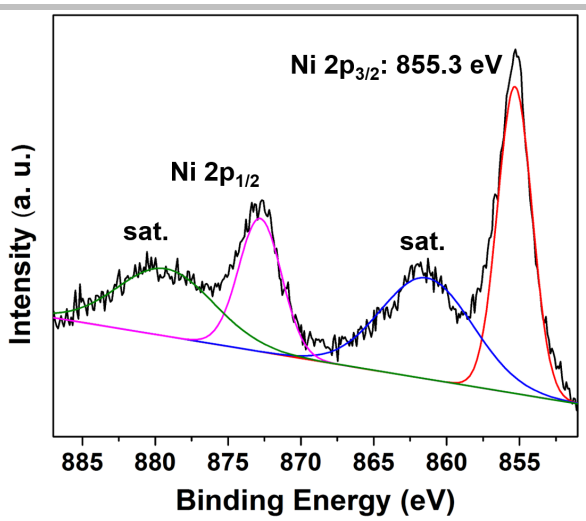

Figure S20. Ni 2p spectrum of recycled MOF-NiH. The Ni $2p_{3/2}$ peak at 855.3 eV indicated the +2 oxidation state of Ni in the recovered catalyst, which was unchanged compared with the pristine MOF-NiH.

4.4.3 TEM of recycled MOF-NiH

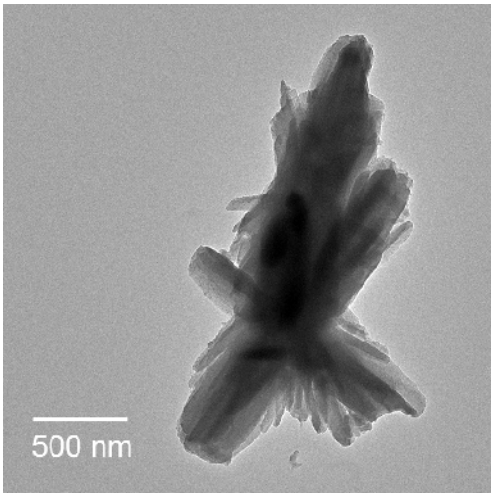

Figure S21. TEM image of recycled MOF-NiH. The nanoscrystal morphology was unchanged after catalytic reaction.

5. GC graphs and Peak Assignments of Catalytic Reaction Products

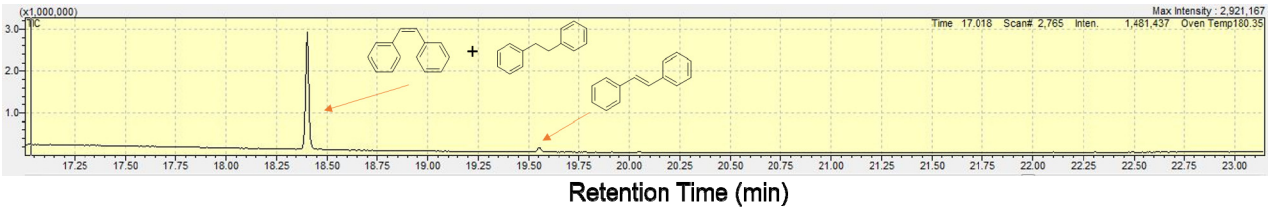

Figure S22. GC graph and assignment of peaks of MOF-NiH-catalyzed semi-hydrogenation of **1a**.

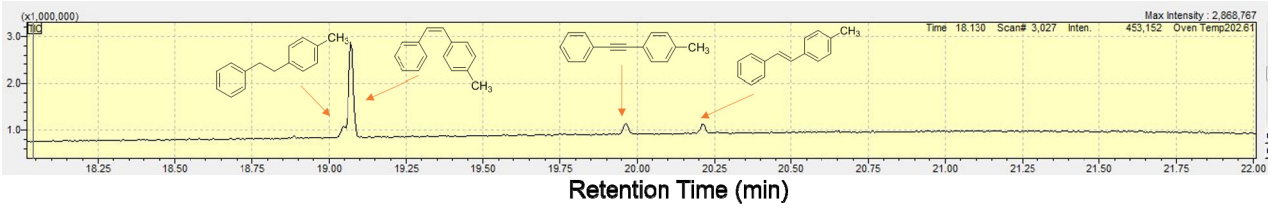

Figure S23. GC graph and assignment of peaks of MOF-NiH-catalyzed semi-hydrogenation of **1b**.

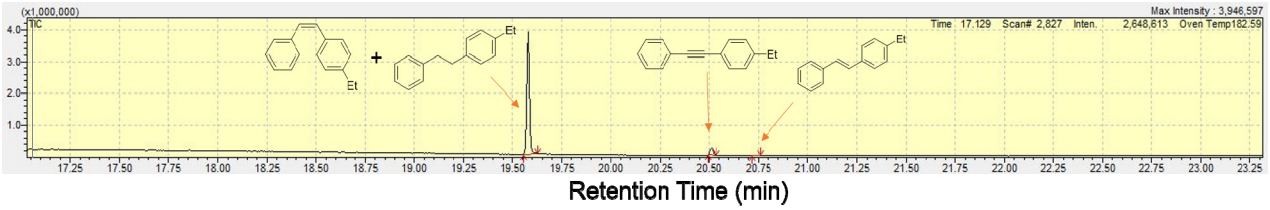

Figure S24. GC graph and assignment of peaks of MOF-NiH-catalyzed semi-hydrogenation of **1c**.

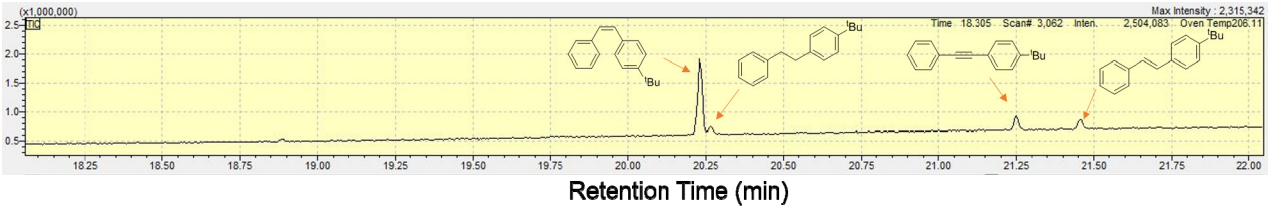

Figure S25. GC graph and assignment of peaks of MOF-NiH-catalyzed semi-hydrogenation of **1d**.

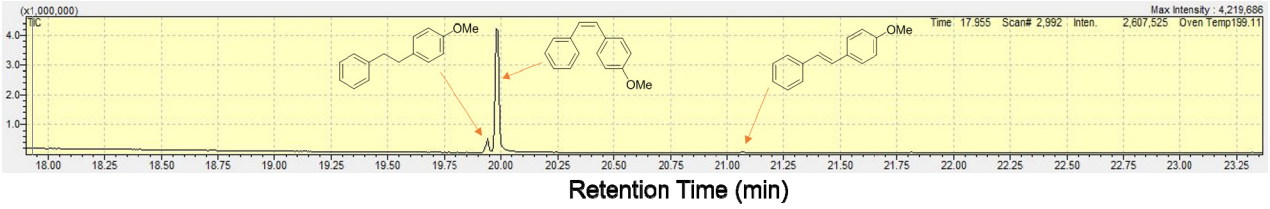

Figure S26. GC graph and assignment of peaks of MOF-NiH-catalyzed semi-hydrogenation of **1e**..

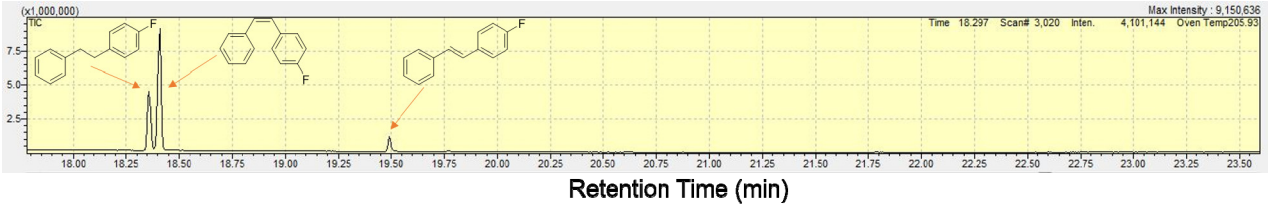

Figure S27. GC graph and assignment of peaks of MOF-NiH-catalyzed semi-hydrogenation of **1f**.

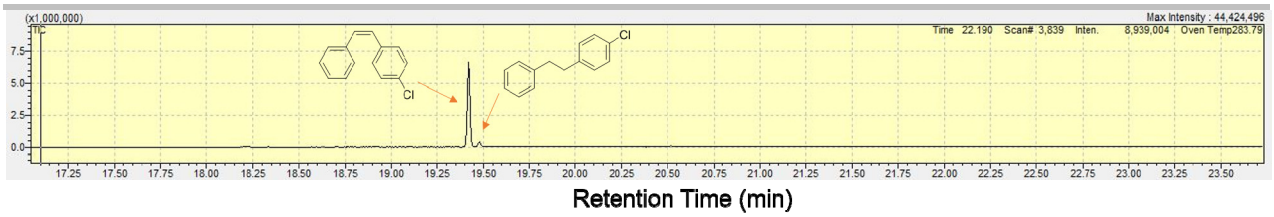

Figure S28. GC graph and assignment of peaks of MOF-NiH-catalyzed semi-hydrogenation of **1g**.

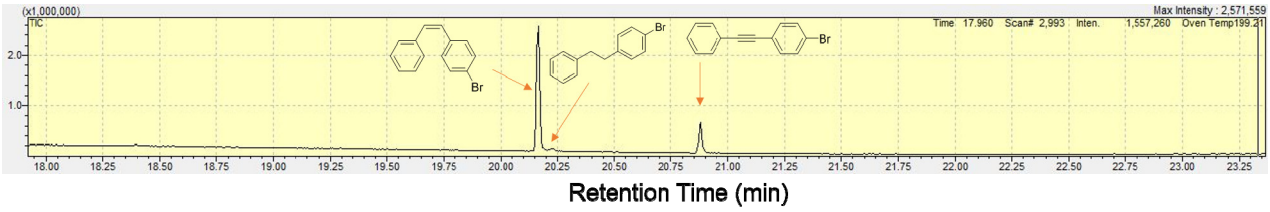

Figure S29. GC graph and assignment of peaks of MOF-NiH-catalyzed semi-hydrogenation of **1h**.

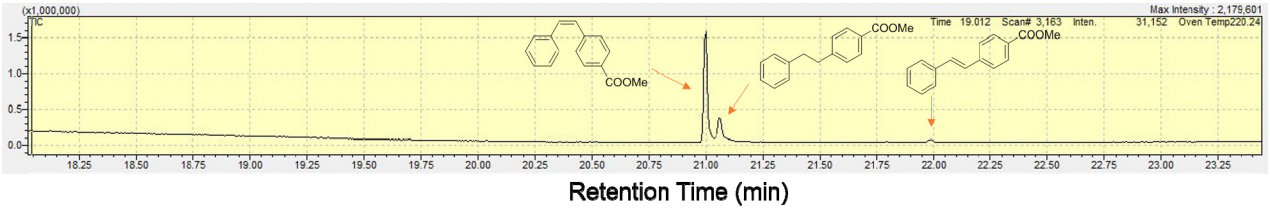

Figure S30. GC graph and assignment of peaks of MOF-NiH-catalyzed semi-hydrogenation of **1i**.

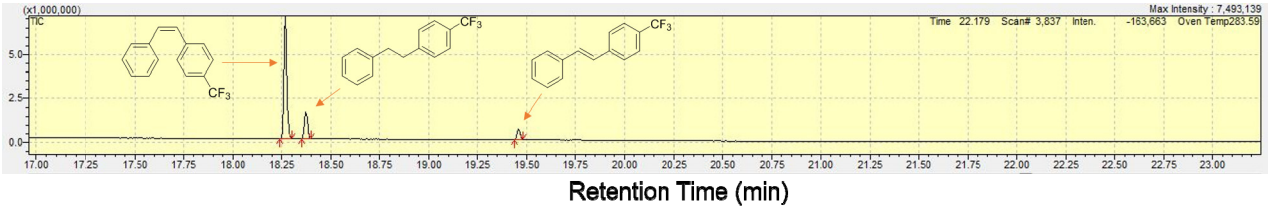

Figure S31. GC graph and assignment of peaks of MOF-NiH-catalyzed semi-hydrogenation of **1j**.

6. Computational Studies

6.1 Computational setup

All density functional theory (DFT) calculations were carried out using Gaussian 16, Revision A.03.[6] The structures of intermediate (IM) species were optimized by using the B3LYP functional and D3(BJ) dispersion correction in gas phase.[7-9] The 6-31G* basis set was used for C, H, O and N, and SDD was used for Ni. Frequency analysis was conducted at the same level of theory to verify the stationary points are minimal or saddle points. The Ni catalyst structure was modeled using the H_2dcbpy ligand with Ni groups linked to the bpy site. In the optimization process, the carboxylate groups were frozen to constrain the structures of linkers connected to SBU. The distance between two adjacent H_2dcbpy ligands were set based on the single crystal structure.[10] The single point energy

calculations on optimized structures were based on def2TZVP basis set, and the SMD solvation model with *n*-hexane as the solvent was employed. The Gibbs free energy of each optimized structure was calculated based on the single point energy and the corresponding thermal correction.[11-12]

6.2 Cartesian coordinates of optimized structures

NiH							
O	-6.08698	3.917198	-0.11013	C	4.780316	3.750317	-0.11599
C	-3.36369	4.417198	-0.44736	C	3.259698	3.66108	-0.13858
C	-1.99186	4.654808	-0.47172	C	0.403704	3.738165	-0.17344
O	-5.48993	-2.66319	-0.10916	C	5.377555	-2.82815	-0.1151
C	-2.44364	-2.55381	0.1285	C	3.886461	-3.12972	-0.12069
N	-1.09274	-2.59403	0.140289	C	1.073513	-3.62663	-0.16748
O	-5.87972	1.631037	-0.10973	H	-4.04478	5.232027	-0.66788
C	-2.9081	2.153052	0.131885	H	-1.63248	5.64866	-0.71784
N	-1.58074	2.385206	0.143408	H	-2.871	-1.59319	0.394329
O	-5.28209	-4.9492	-0.10845	H	-3.20818	1.141254	0.380297
C	-2.54598	-4.85021	-0.47994	H	-3.11971	-5.74283	-0.69906
C	-1.15727	-4.88709	-0.50087	H	-0.65618	-5.81499	-0.75672
O	5.284004	4.949454	-0.13391	H	3.123719	5.747886	-0.65192
C	2.548208	4.854591	-0.4409	H	0.660618	5.821065	-0.7254
C	1.159913	4.891372	-0.47259	H	3.204381	-1.14132	0.404566
O	5.881736	-1.63079	-0.13268	H	2.867823	1.591141	0.41162
C	2.907204	-2.15418	0.15688	H	4.049655	-5.23423	-0.62876
N	1.579634	-2.38634	0.157054	H	1.638227	-5.65091	-0.69898
O	5.492041	2.663533	-0.13353	H	-7.02532	3.644495	-0.10797
C	2.442634	2.553955	0.150204	H	-6.42569	-2.93864	-0.05713
N	1.091564	2.593843	0.15151	H	6.42913	2.939037	-0.11802
O	6.088893	-3.91695	-0.13207	H	7.026649	-3.64417	-0.16373
C	3.366949	-4.41922	-0.41444	H	-1.04389	-0.10659	0.984342
C	1.995413	-4.65661	-0.45139	H	1.035633	0.105649	0.993842
C	-5.37574	2.829002	-0.12793	Ni	0.123737	-1.14807	0.596459
C	-3.885	3.128502	-0.15436	Ni	-0.12851	1.146982	0.595013
C	-1.0724	3.625956	-0.17545				
C	-4.77831	-3.75047	-0.12662				
C	-3.25883	-3.65916	-0.1723				
C	-0.40282	-3.73708	-0.18438				

IM-1				IM-2			
O	-6.08698	3.917198	-0.11013	O	-6.08696	3.917207	-0.11013
C	-3.36207	4.400184	0.243506	C	-3.3642	4.43786	0.094458
C	-1.98994	4.631314	0.295504	C	-1.98993	4.67351	0.074915
O	-5.48993	-2.66319	-0.10916	O	-5.48996	-2.66321	-0.10915
C	-2.44244	-2.55257	-0.39454	C	-2.45064	-2.54435	0.153683
N	-1.09228	-2.59076	-0.38407	N	-1.0989	-2.56562	0.200761
O	-5.87972	1.631037	-0.10973	O	-5.87975	1.631048	-0.10973
C	-2.9051	2.165349	-0.44062	C	-2.93022	2.163886	-0.4444

N	-1.57689	2.391191	-0.41624	N	-1.59989	2.395235	-0.4861
O	-5.28209	-4.9492	-0.10845	O	-5.28209	-4.9492	-0.10845
C	-2.5494	-4.83768	0.251547	C	-2.52932	-4.84335	-0.44127
C	-1.16167	-4.86841	0.306489	C	-1.14612	-4.86801	-0.43843
O	5.284004	4.949454	-0.13391	O	5.283997	4.949457	-0.13391
C	2.551399	4.831879	0.290933	C	2.538668	4.871768	-0.02753
C	1.162809	4.862797	0.334575	C	1.148441	4.915622	-0.06403
O	5.881736	-1.63079	-0.13268	O	5.881766	-1.6308	-0.13268
C	2.909751	-2.16361	-0.41571	C	2.942665	-2.1901	0.283698
N	1.581759	-2.38958	-0.4018	N	1.615358	-2.42321	0.331807
O	5.492041	2.663533	-0.13353	O	5.49206	2.663545	-0.13352
C	2.447648	2.552849	-0.37661	C	2.435277	2.512868	-0.30004
N	1.097315	2.591632	-0.3766	N	1.08425	2.554916	-0.35601
O	6.088893	-3.91695	-0.13207	O	6.088891	-3.91695	-0.13207
C	3.362773	-4.39693	0.276961	C	3.35633	-4.40999	-0.46542
C	1.990622	-4.62893	0.316734	C	1.988501	-4.63393	-0.48101
C	-5.37574	2.829002	-0.12793	C	-5.3757	2.828962	-0.12793
C	-3.88489	3.127517	-0.11545	C	-3.88697	3.14318	-0.1611
C	-1.06839	3.613731	-0.03281	C	-1.08494	3.634936	-0.21814
C	-4.77831	-3.75047	-0.12662	C	-4.77823	-3.75043	-0.12663
C	-3.25915	-3.65664	-0.09314	C	-3.25929	-3.65036	-0.15327
C	-0.40546	-3.72312	-0.02119	C	-0.39227	-3.71042	-0.11372
C	4.780316	3.750317	-0.11599	C	4.780277	3.750281	-0.116
C	3.262177	3.65433	-0.06064	C	3.248001	3.651181	-0.13655
C	0.408988	3.721625	-0.0121	C	0.406099	3.731922	-0.21838
C	5.377555	-2.82815	-0.1151	C	5.37747	-2.82812	-0.11511
C	3.887622	-3.12478	-0.08153	C	3.897744	-3.13668	-0.09874
C	1.070601	-3.61305	-0.02341	C	1.072454	-3.62246	-0.09004
H	-4.04294	5.205532	0.49692	H	-4.03948	5.253281	0.327265
H	-1.63149	5.611618	0.592426	H	-1.62159	5.667309	0.306675
H	-2.86752	-1.5935	-0.66512	H	-2.90032	-1.58835	0.397519
H	-3.20152	1.165931	-0.73797	H	-3.24052	1.144289	-0.64676
H	-3.12458	-5.72673	0.480754	H	-3.09272	-5.7421	-0.66227
H	-0.66292	-5.78843	0.59384	H	-0.63464	-5.79524	-0.67571
H	3.124823	5.719568	0.530131	H	3.112967	5.783935	0.081559
H	0.662106	5.780343	0.626368	H	0.644779	5.872141	0.028871
H	3.208928	-1.16587	-0.71585	H	3.258152	-1.19568	0.587245
H	2.874868	1.596975	-0.65473	H	2.861592	1.519689	-0.39915
H	4.042135	-5.20176	0.536421	H	4.027671	-5.20757	-0.76428
H	1.630132	-5.60897	0.612098	H	1.617264	-5.59956	-0.80865
H	-7.02519	3.646025	-0.07536	H	-7.02612	3.64971	-0.06535
H	-6.42605	-2.94069	-0.14283	H	-6.42506	-2.94115	-0.05888
H	6.426113	2.941349	-0.20277	H	6.430114	2.935956	-0.15243
H	7.027742	-3.64582	-0.13089	H	7.026185	-3.64508	-0.18038
H	-1.03526	-0.10618	-1.22275	H	0.511557	-0.33251	-0.94444
H	1.047079	0.1024	-1.21558	Ni	0.229655	-1.04281	0.722142
Ni	0.128313	-1.14599	-0.82494	Ni	-0.23129	1.008857	-0.48174
Ni	-0.11995	1.145919	-0.82745	C	-0.53997	0.396925	1.914388

C	-0.51574	-0.22412	2.485633	C	0.494687	1.247397	2.551695
C	0.587816	0.285237	2.492341	C	1.764461	0.711405	2.842615
C	-1.81287	-0.80592	2.536807	C	0.321726	2.633657	2.739569
C	-2.94018	-0.06051	2.143281	C	2.811007	1.512896	3.296861
C	-1.99208	-2.12134	3.003451	H	1.925998	-0.35723	2.709272
C	-4.21495	-0.61368	2.212825	C	1.368071	3.438771	3.180522
H	-2.79769	0.95132	1.785109	H	-0.64432	3.074988	2.522009
C	-3.27208	-2.66159	3.093483	C	2.620879	2.886129	3.460102
H	-1.12313	-2.70257	3.294568	H	3.778067	1.065719	3.510879
C	-4.38387	-1.91085	2.704564	H	1.209389	4.507762	3.296739
H	-5.06509	-0.03565	1.863391	H	3.43791	3.518925	3.79462
H	-3.40217	-3.67664	3.457548	C	-1.8692	0.461917	2.192282
H	-5.3777	-2.34325	2.766099	H	-2.52724	-0.11581	1.545476
C	1.887941	0.859294	2.551859	C	-2.63938	1.202598	3.203995
C	3.009528	0.113191	2.142555	C	-3.99687	1.461505	2.930314
C	2.077237	2.16526	3.040202	C	-2.11973	1.638039	4.437852
C	4.287878	0.656778	2.216717	C	-4.789	2.177785	3.825177
H	2.859213	-0.89162	1.768279	H	-4.43202	1.098848	2.002977
C	3.361105	2.696056	3.133605	C	-2.91499	2.344912	5.33477
H	1.213303	2.74705	3.34479	H	-1.09028	1.414368	4.691078
C	4.466756	1.94521	2.727778	C	-4.25	2.630305	5.03038
H	5.132605	0.078249	1.855259	H	-5.83122	2.370878	3.583903
H	3.499052	3.703996	3.514303	H	-2.4935	2.669484	6.282502
H	5.46354	2.370733	2.792079	H	-4.86543	3.18359	5.734386

7. NMR Spectra

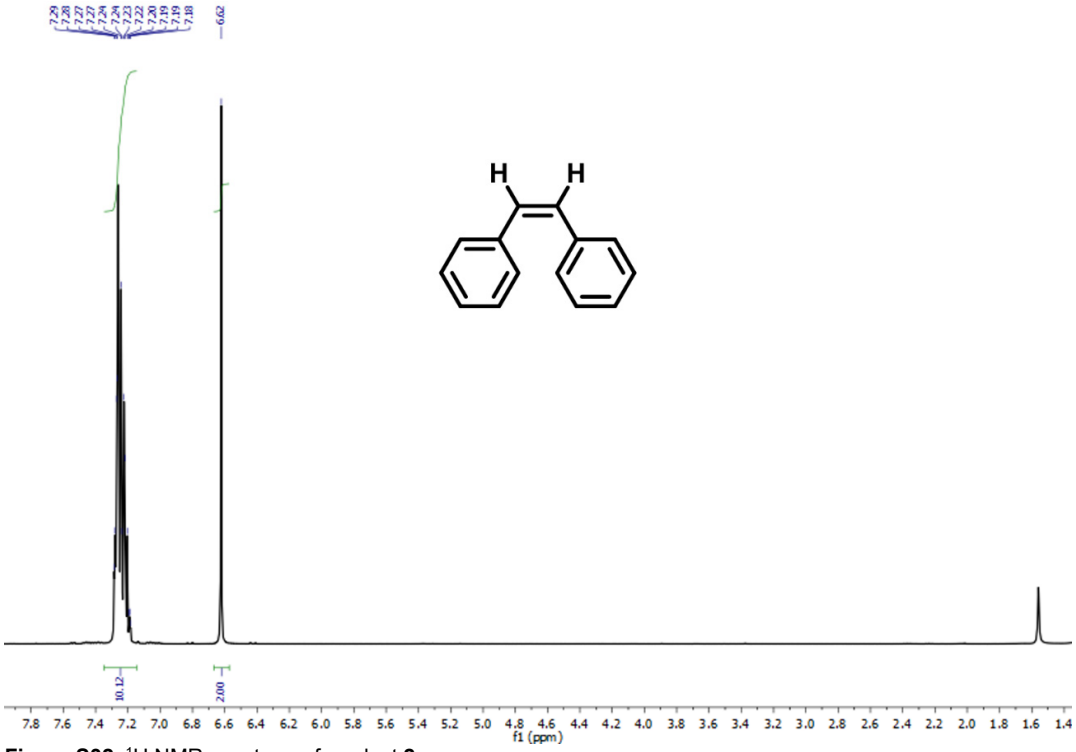

Figure S32. ^{1}H NMR spectrum of product **2a**.

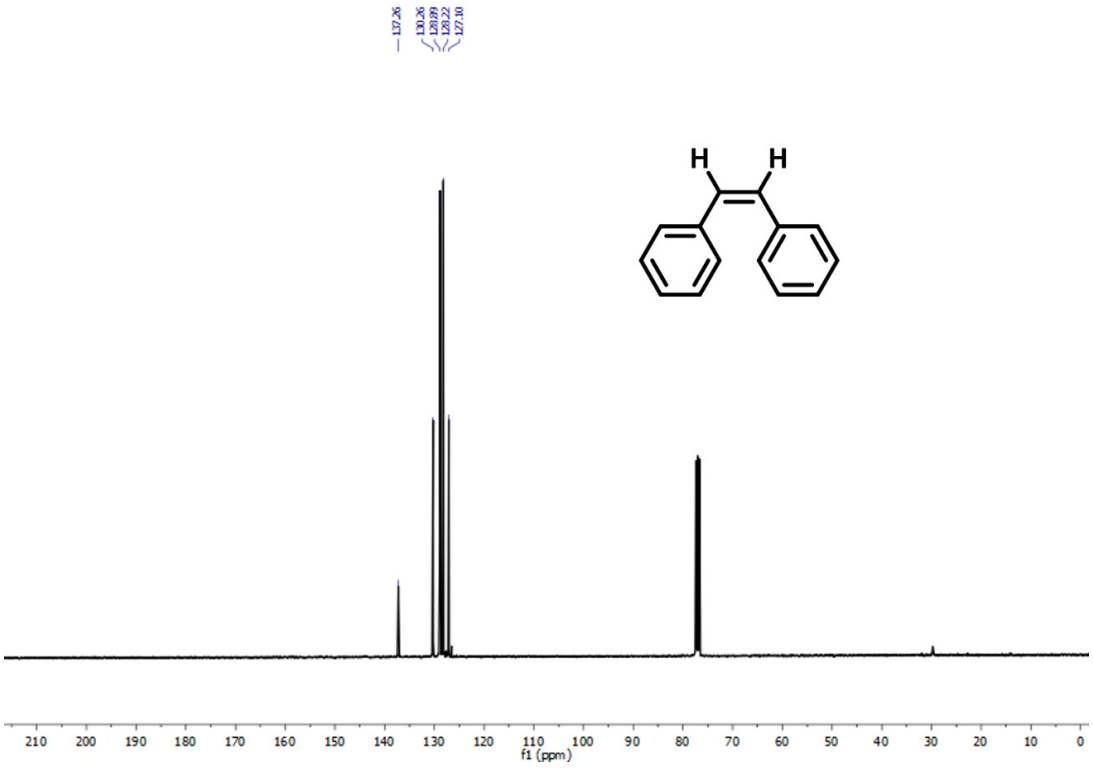

Figure S33. ^{13}C NMR spectrum of product **2a**.

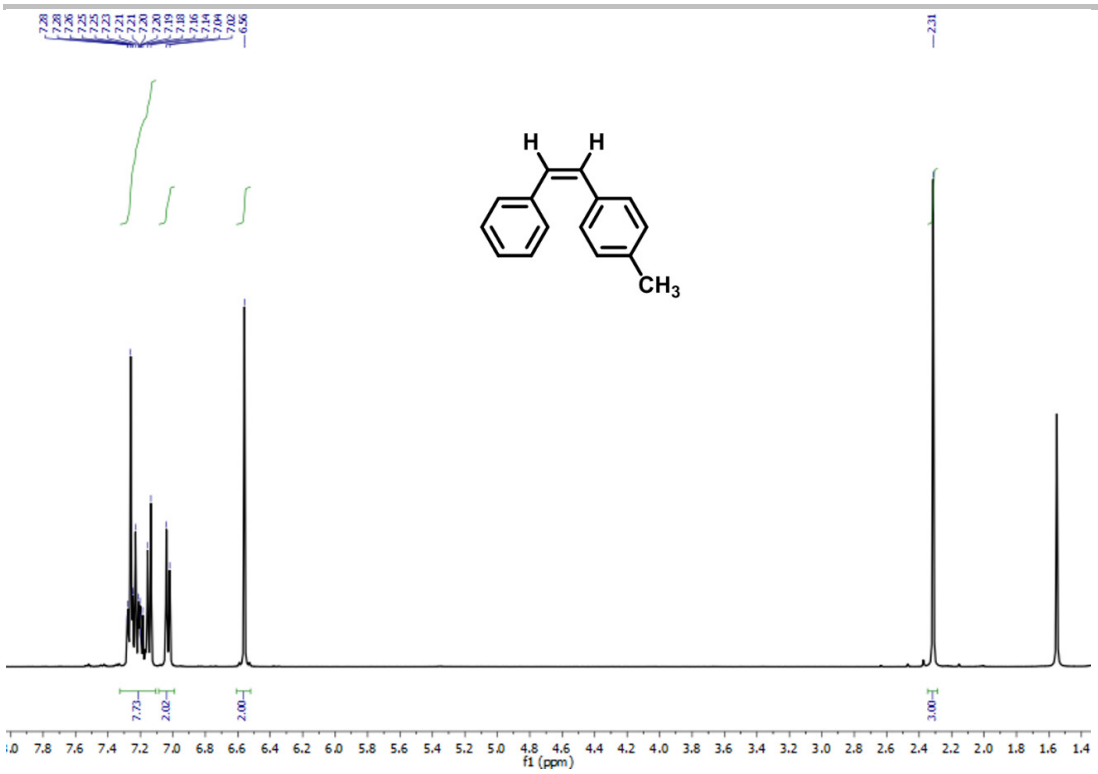

Figure S34. ^{1}H NMR spectrum of product **2b**.

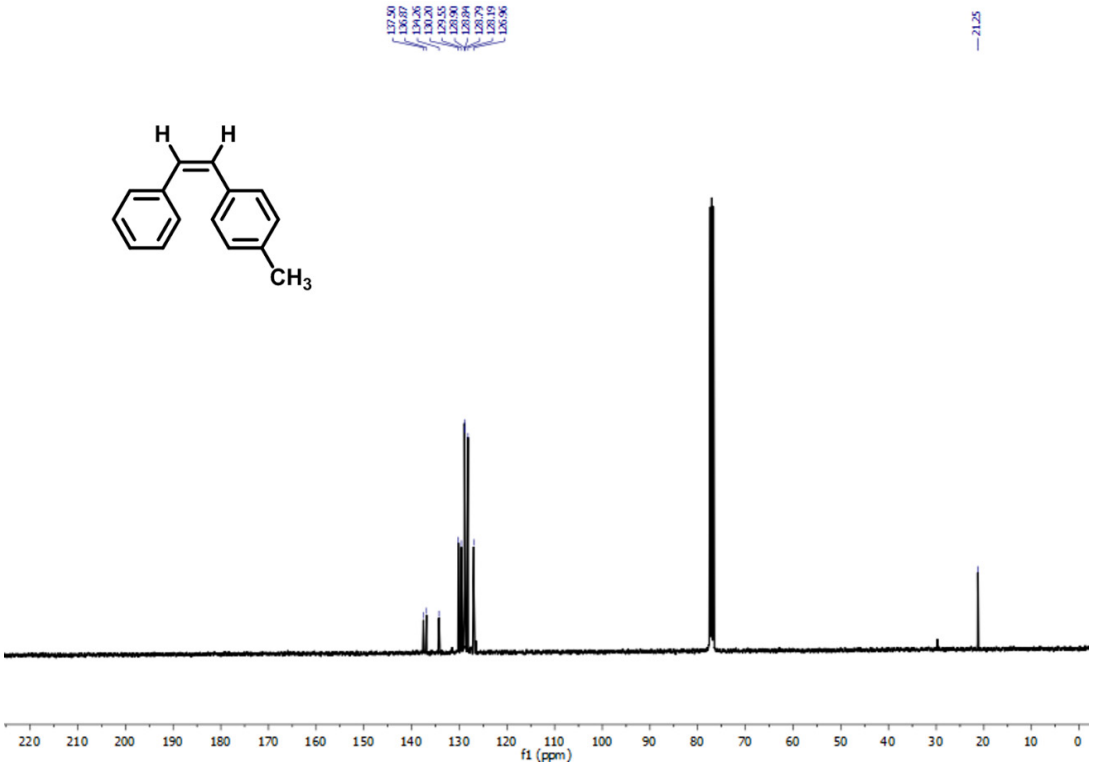

Figure S35. ^{13}C NMR spectrum of product **2b**.

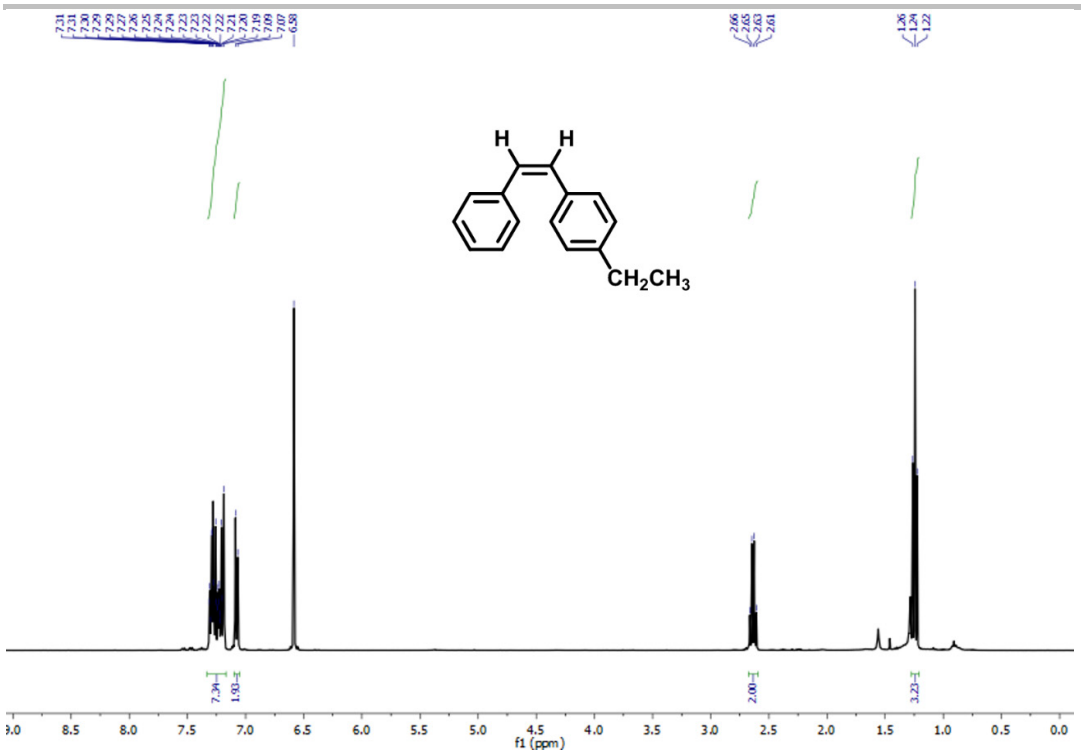

Figure S36. ^{1}H NMR spectrum of product **2c**.

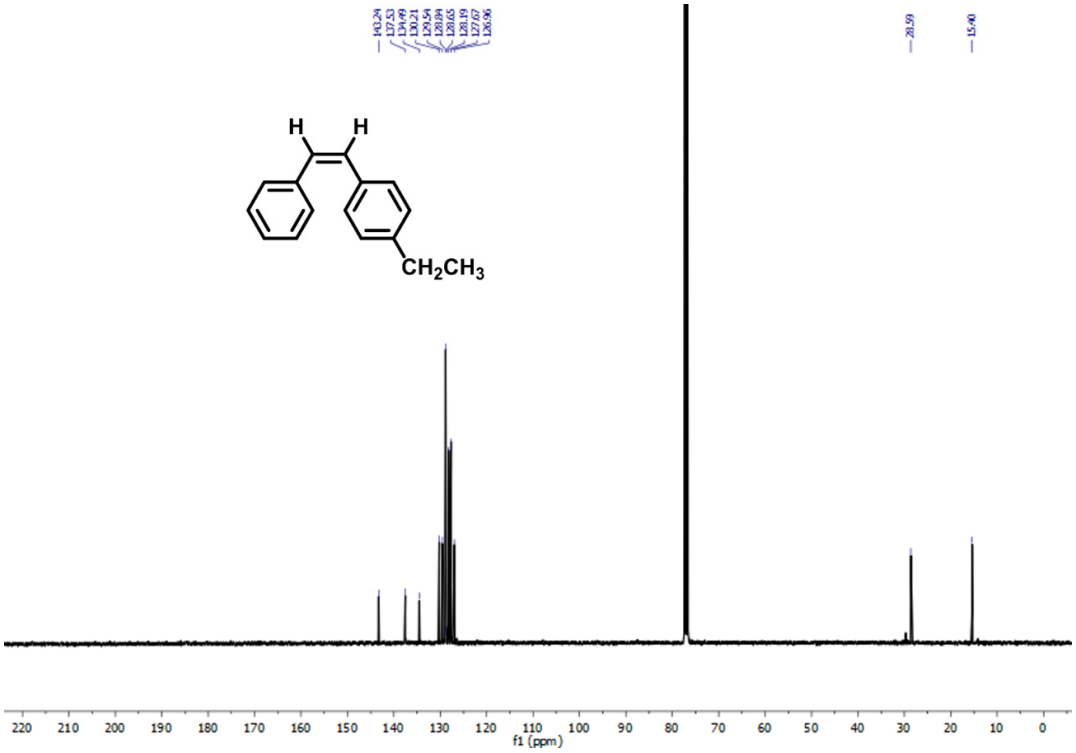

Figure S37. ^{13}C NMR spectrum of product **2c**.

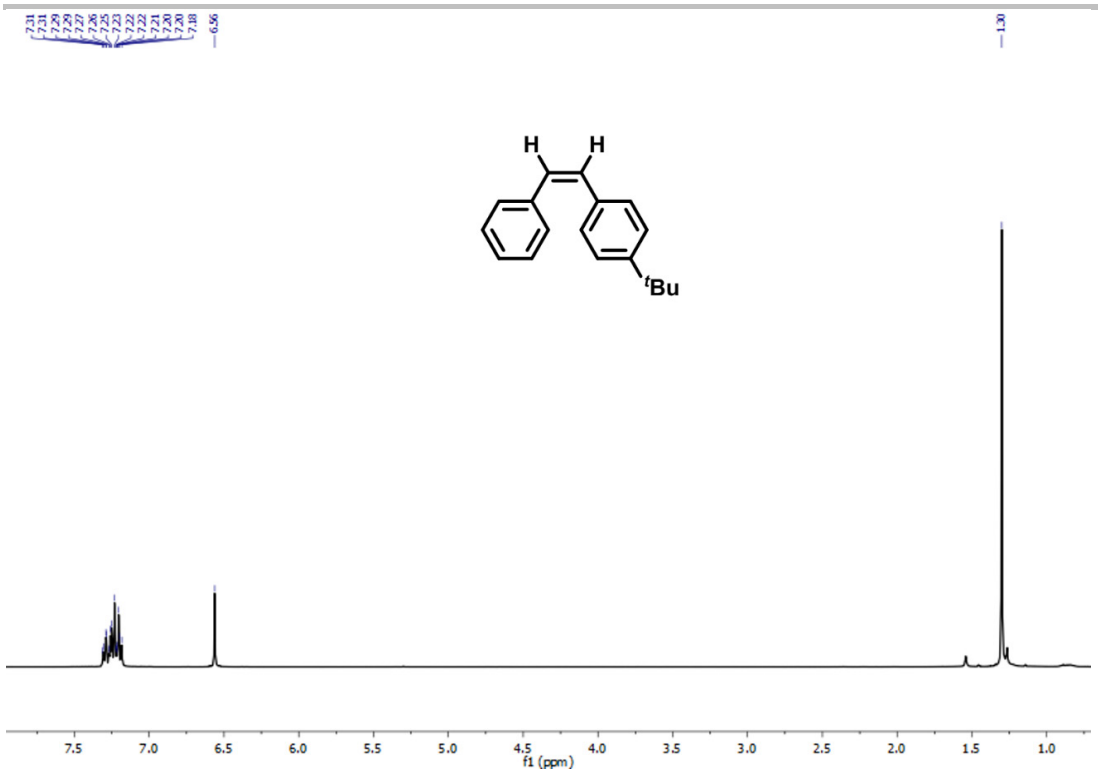

Figure S38. ^{1}H NMR spectrum of product **2d**.

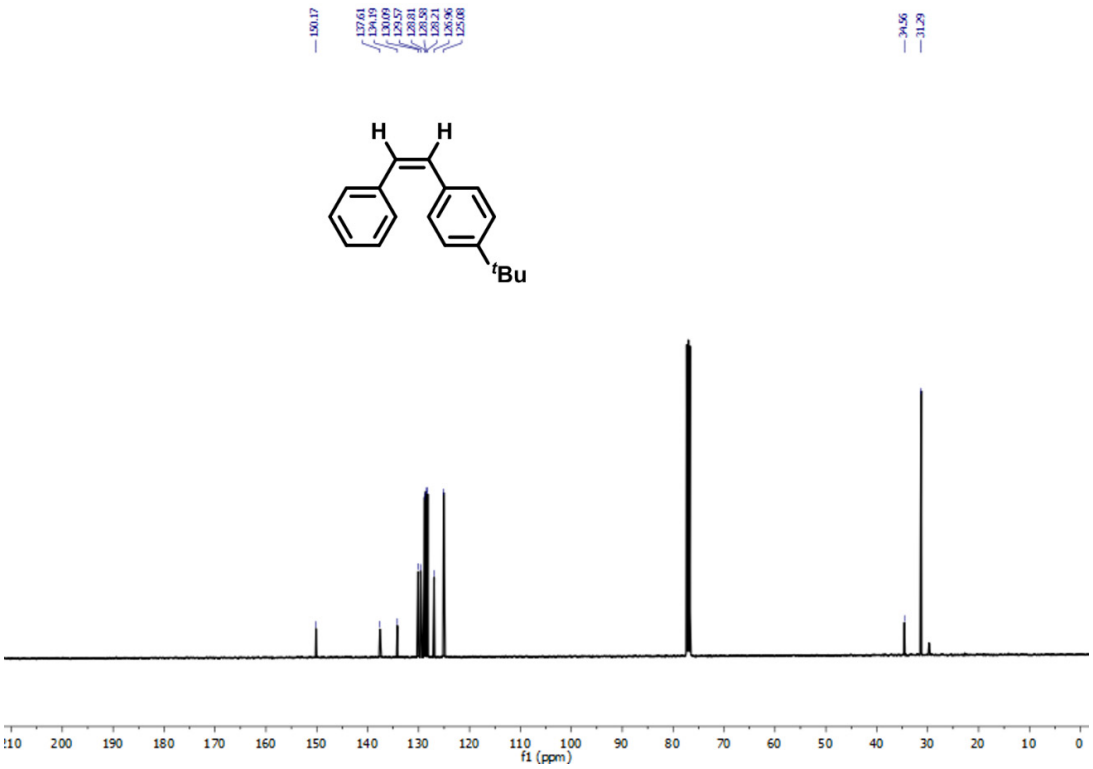

Figure S39. ^{13}C NMR spectrum of product **2d**.

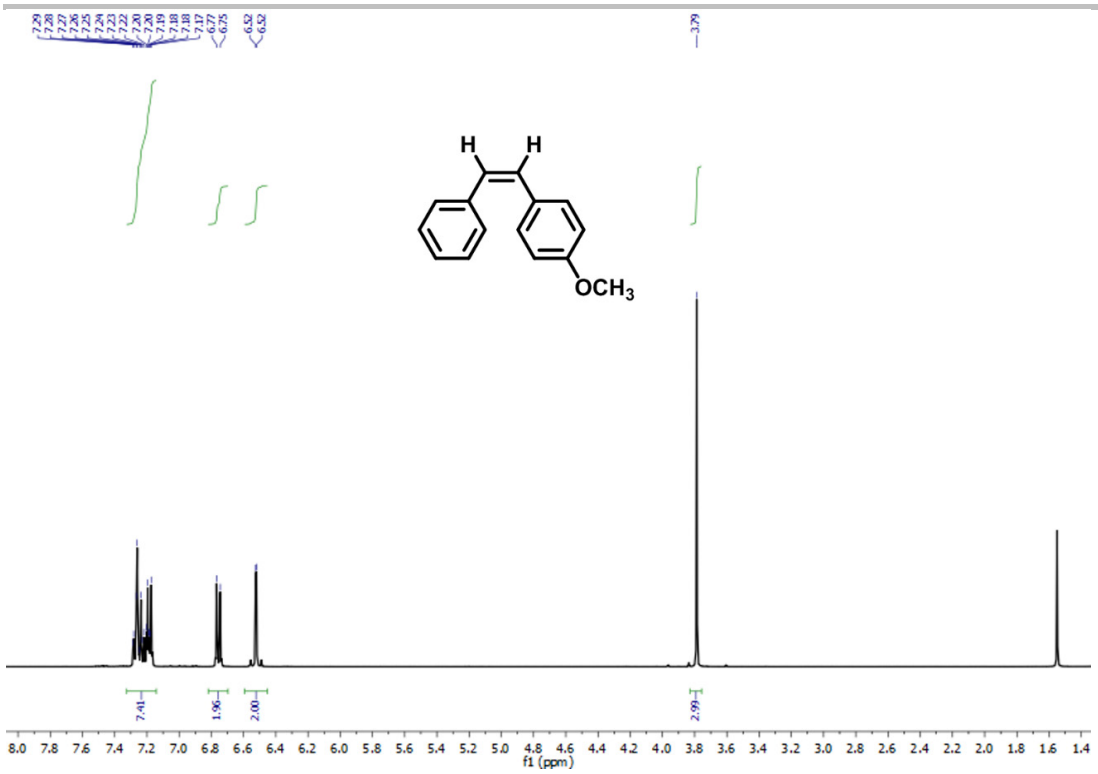

Figure S40. ^{1}H NMR spectrum of product **2e**.

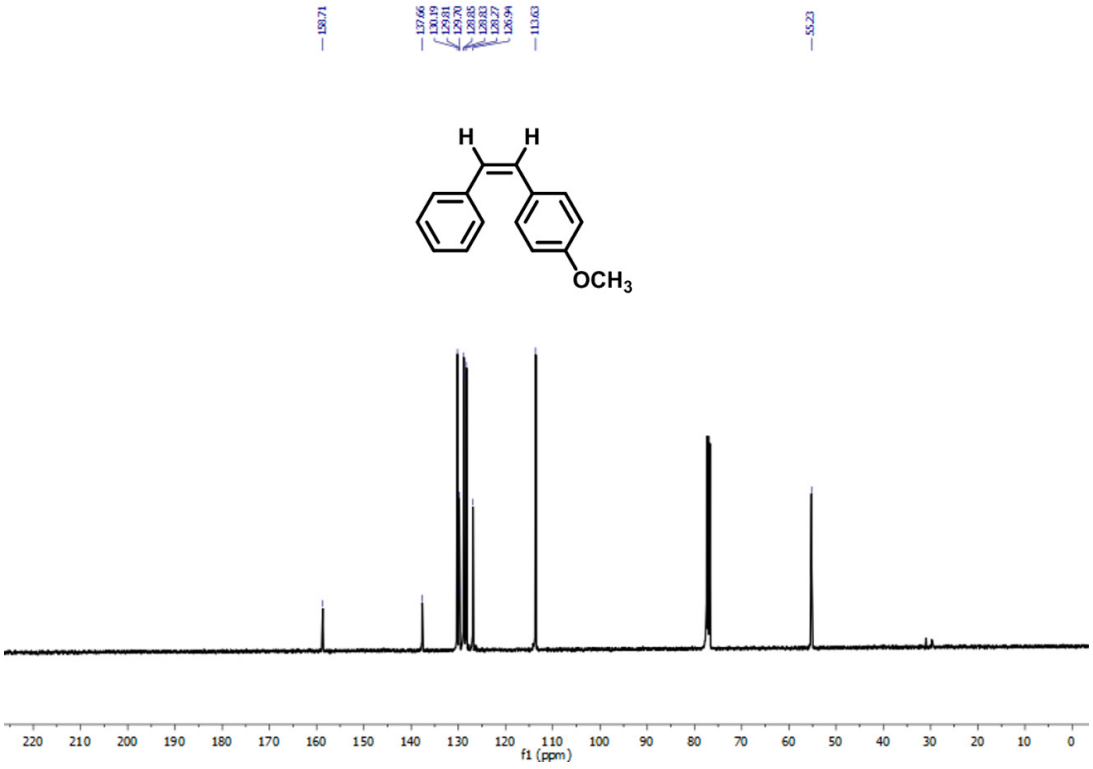

Figure S41. ^{13}C NMR spectrum of product **2e**.

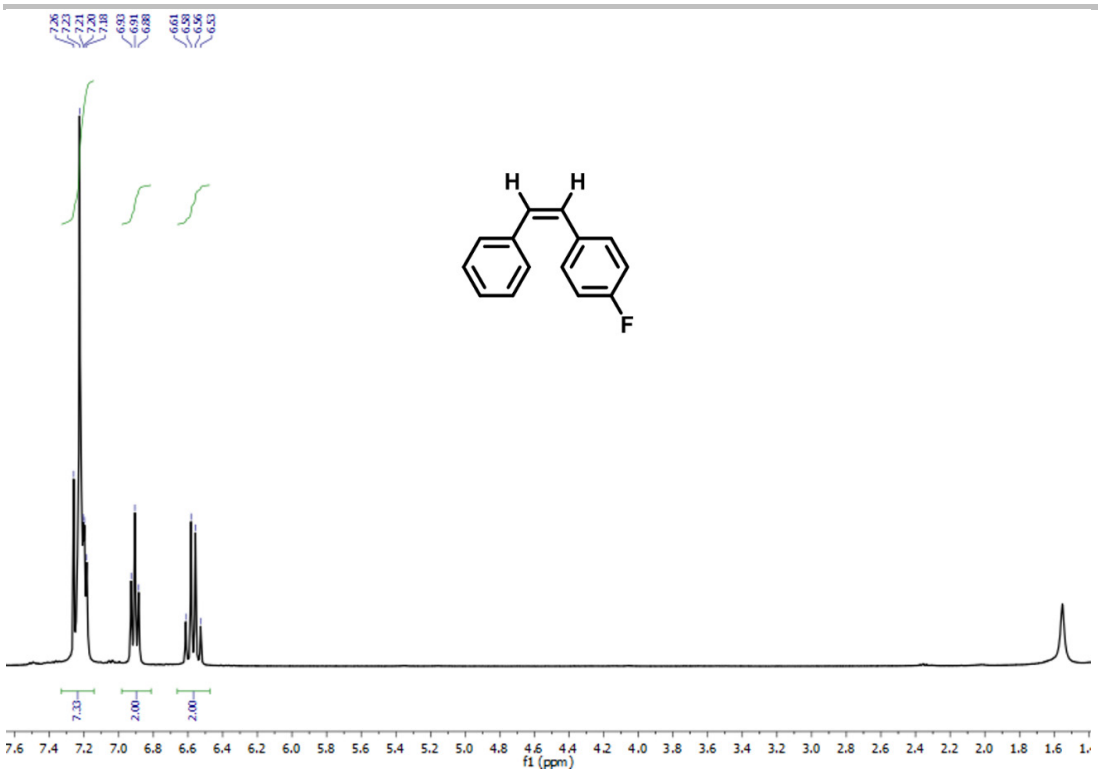

Figure S42. ^{1}H NMR spectrum of product **2f**.

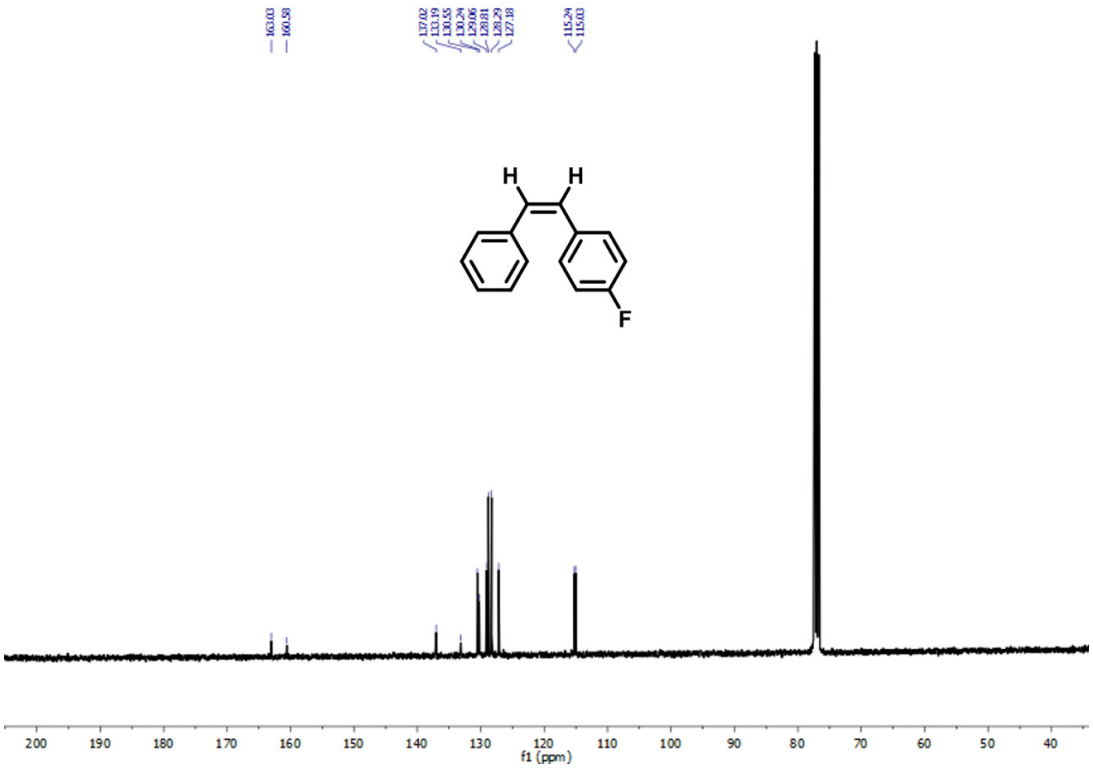

Figure S43. ^{13}C NMR spectrum of product **2f**.

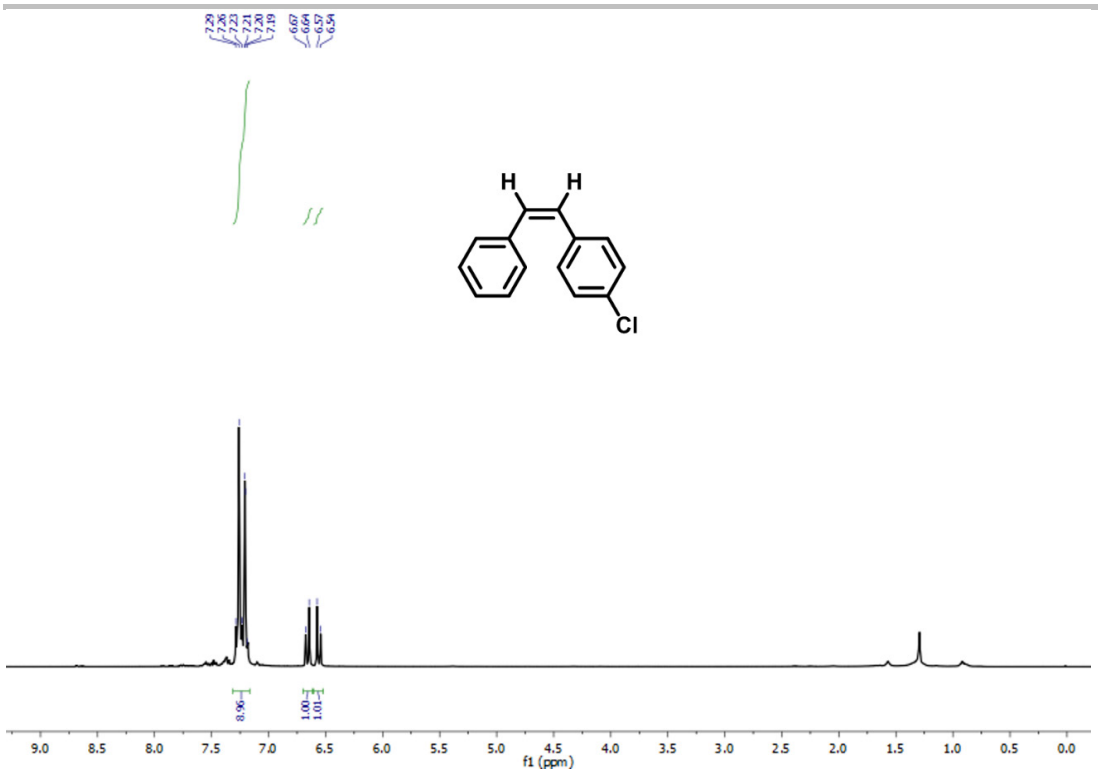

Figure S44. ^{1}H NMR spectrum of product **2g**.

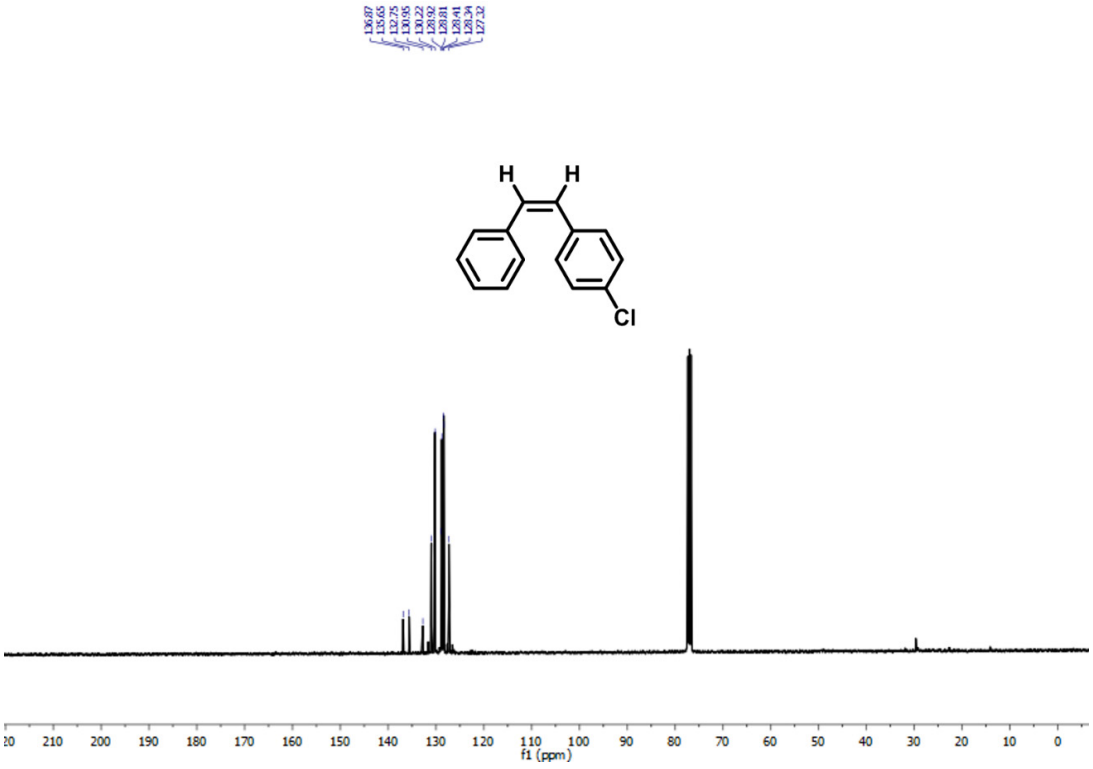

Figure S45. ^{13}C NMR spectrum of product **2g**.

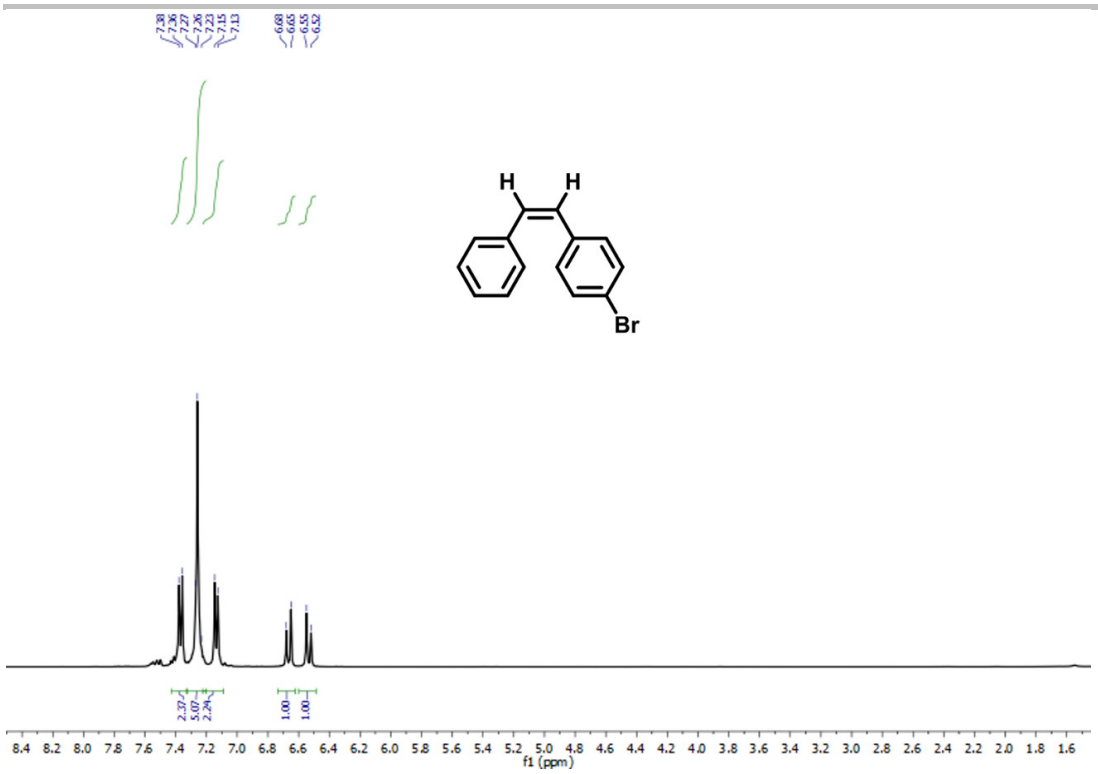

Figure S46. ^{1}H NMR spectrum of product **2h**.

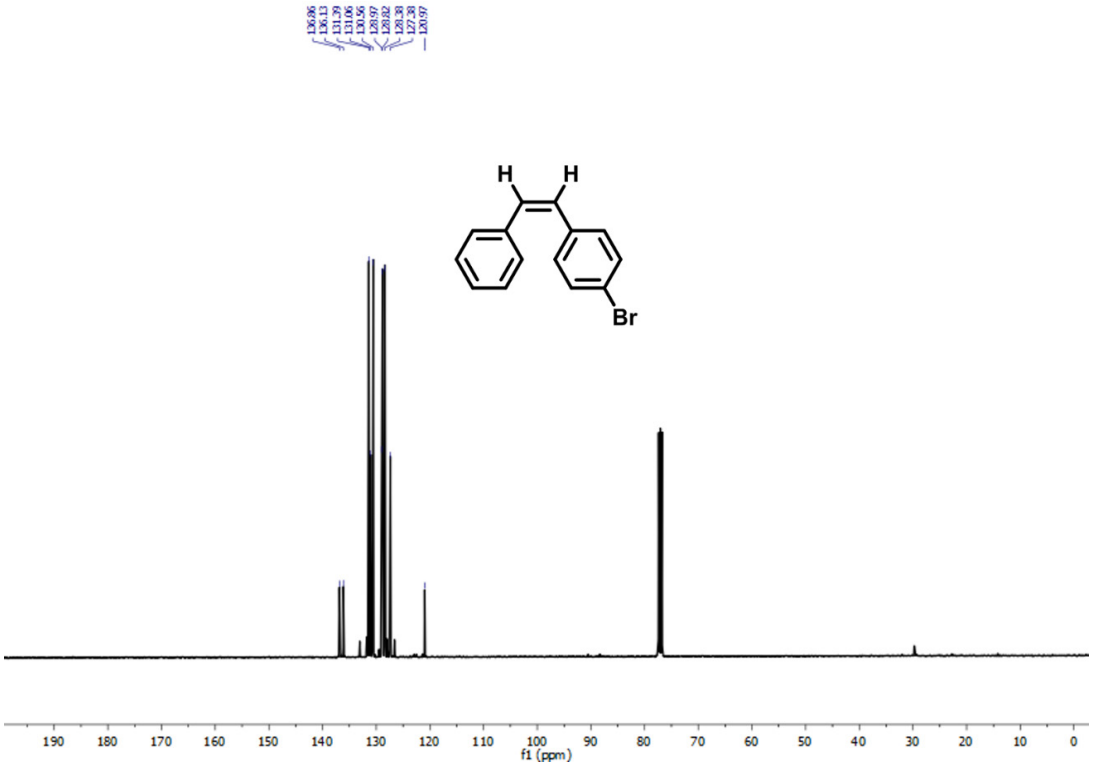

Figure S47. ^{13}C NMR spectrum of product **2h**.

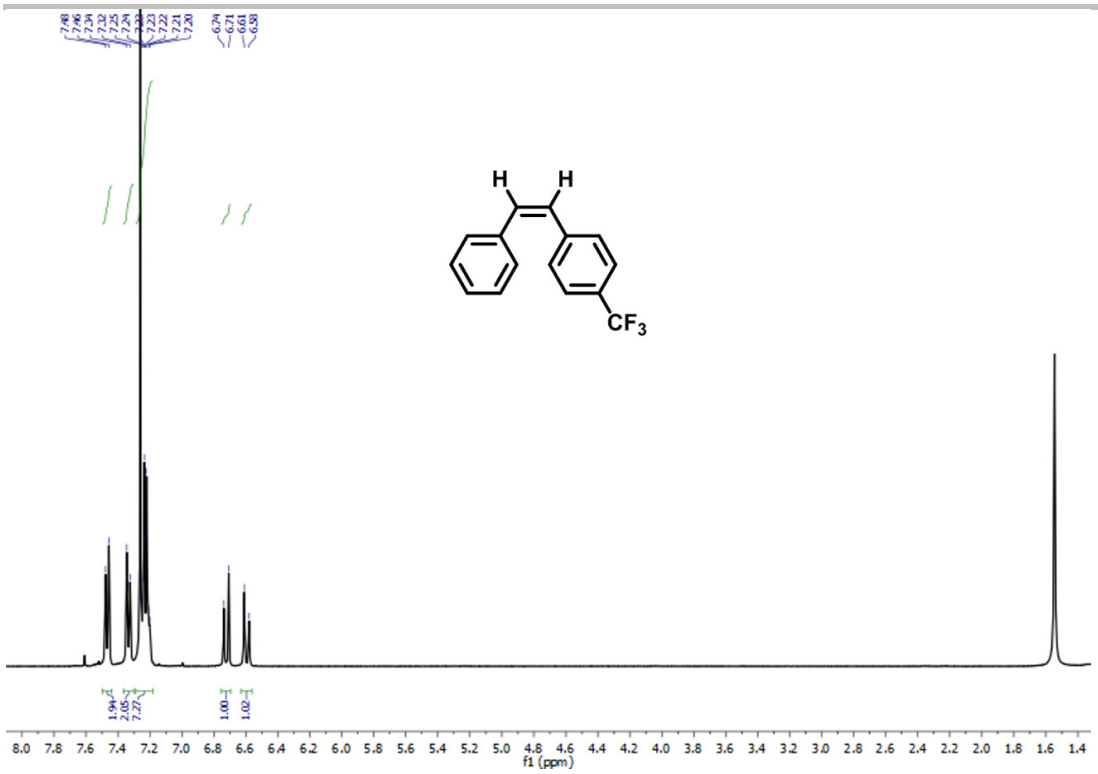

Figure S48. ^{1}H NMR spectrum of product **2j**.

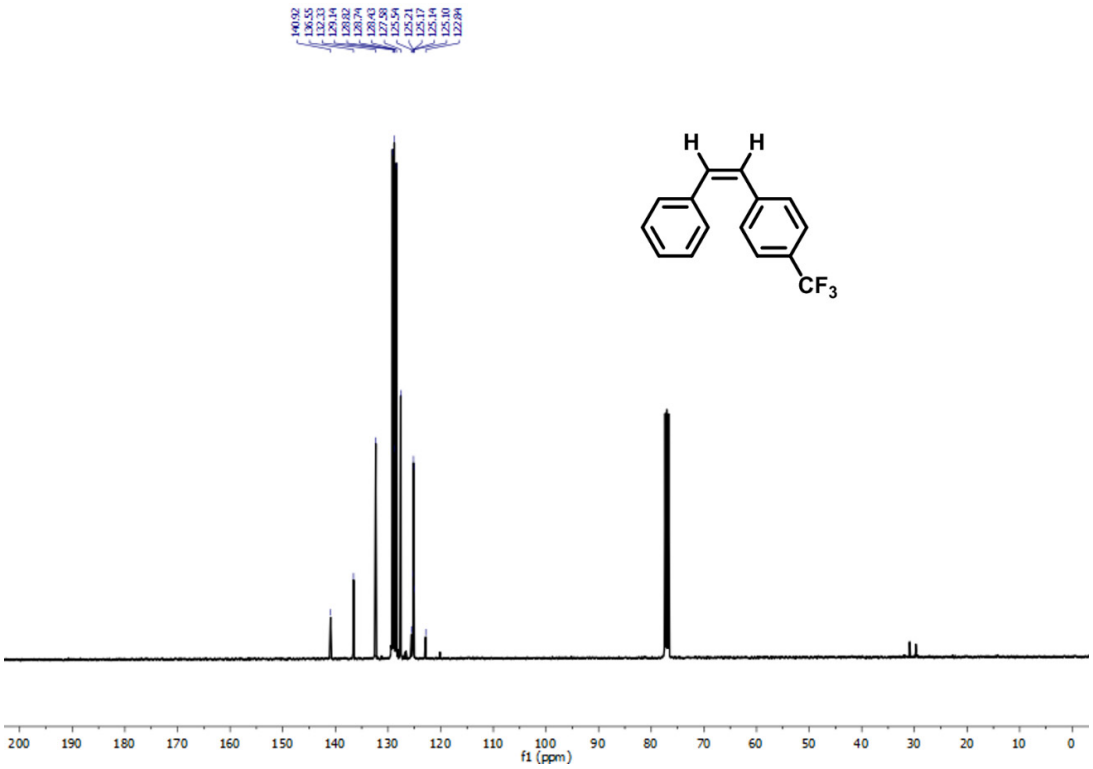

Figure S49. ^{13}C NMR spectrum of product **2j**.

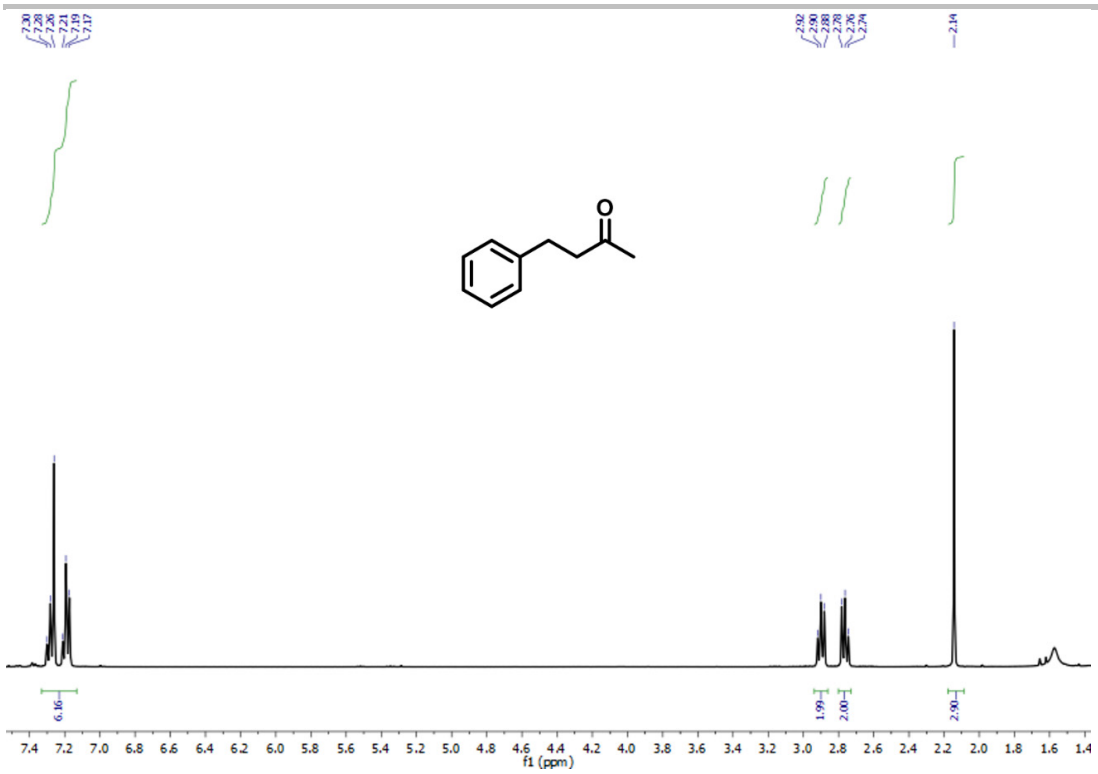

Figure S50. ^{1}H NMR spectrum of product **6b**.

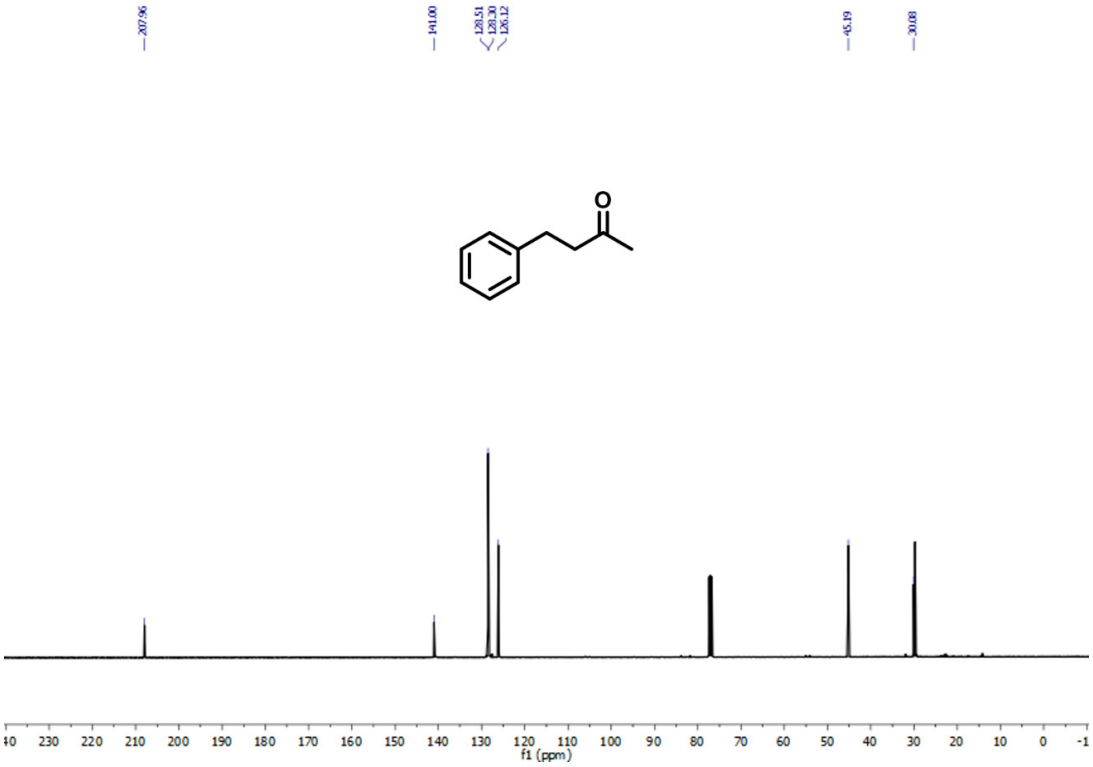

Figure S51. ^{13}C NMR spectrum of product **6b**.

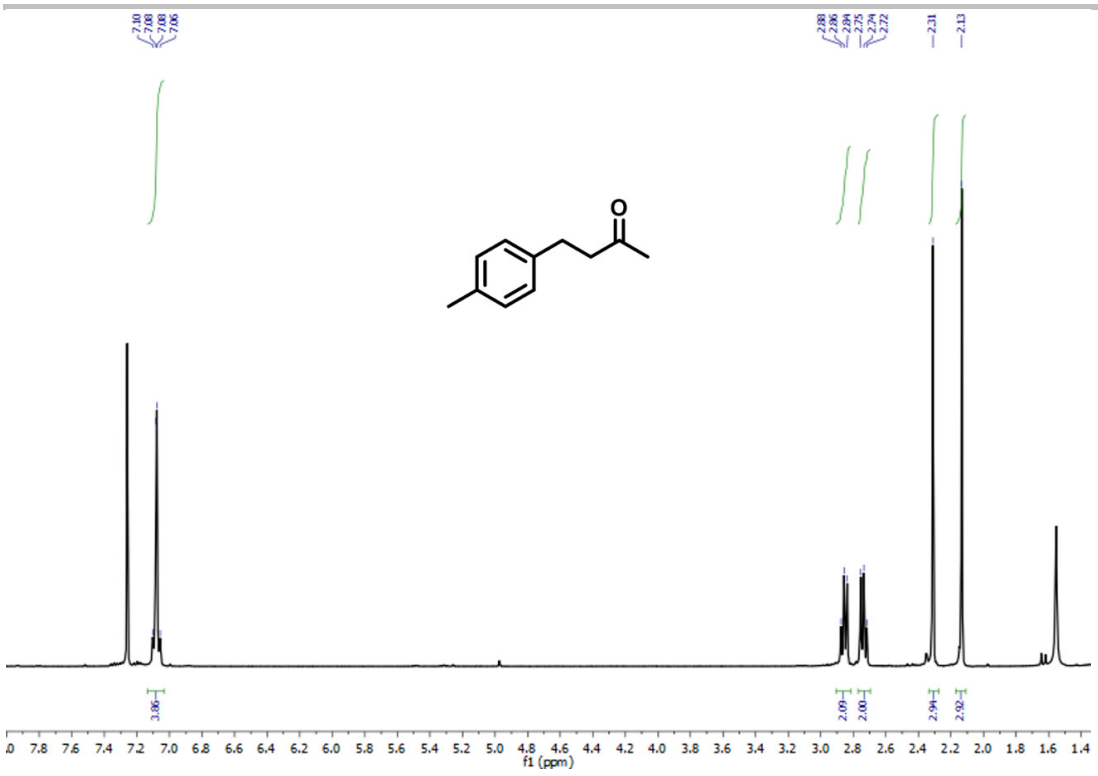

Figure S52. ^{1}H NMR spectrum of product **6c**.

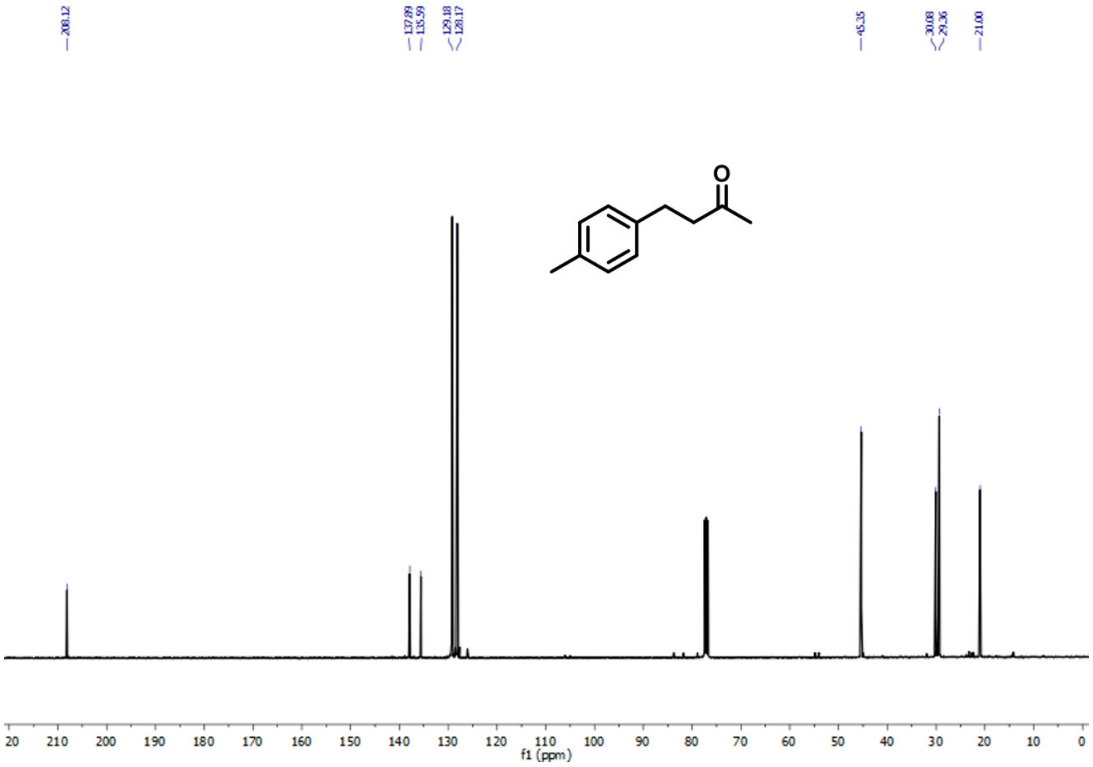

Figure S53. ^{13}C NMR spectrum of product **6c**.

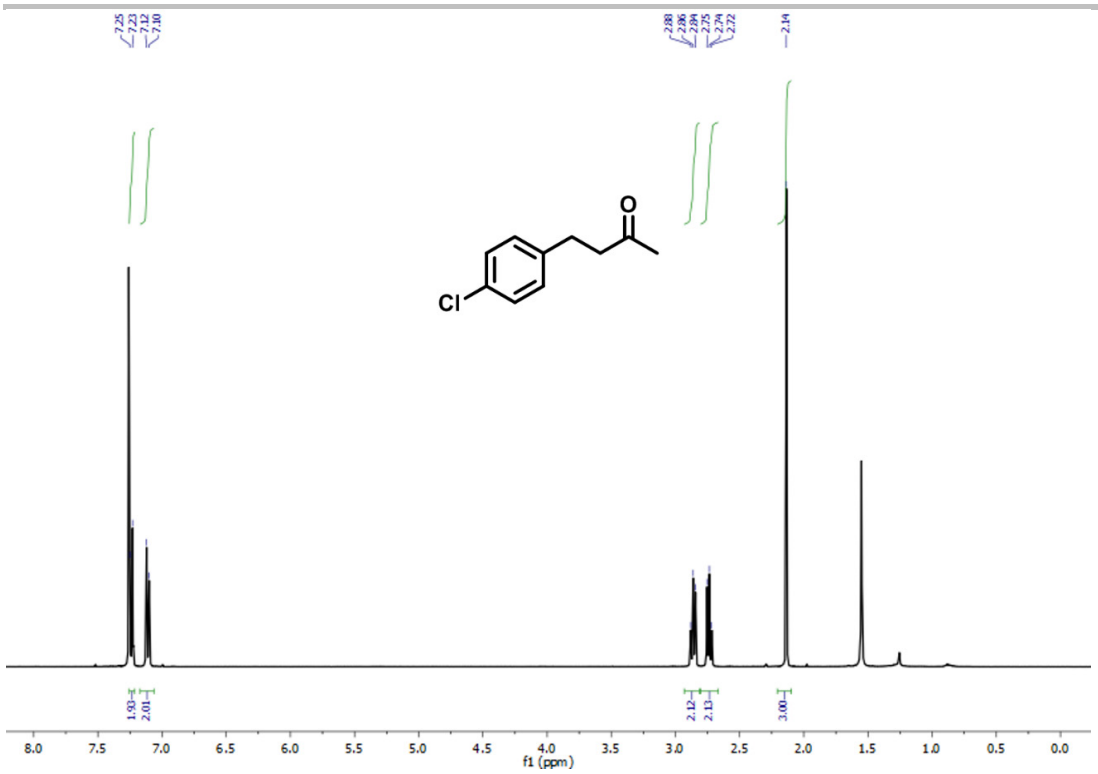

Figure S54. ^{1}H NMR spectrum of product **6d**.

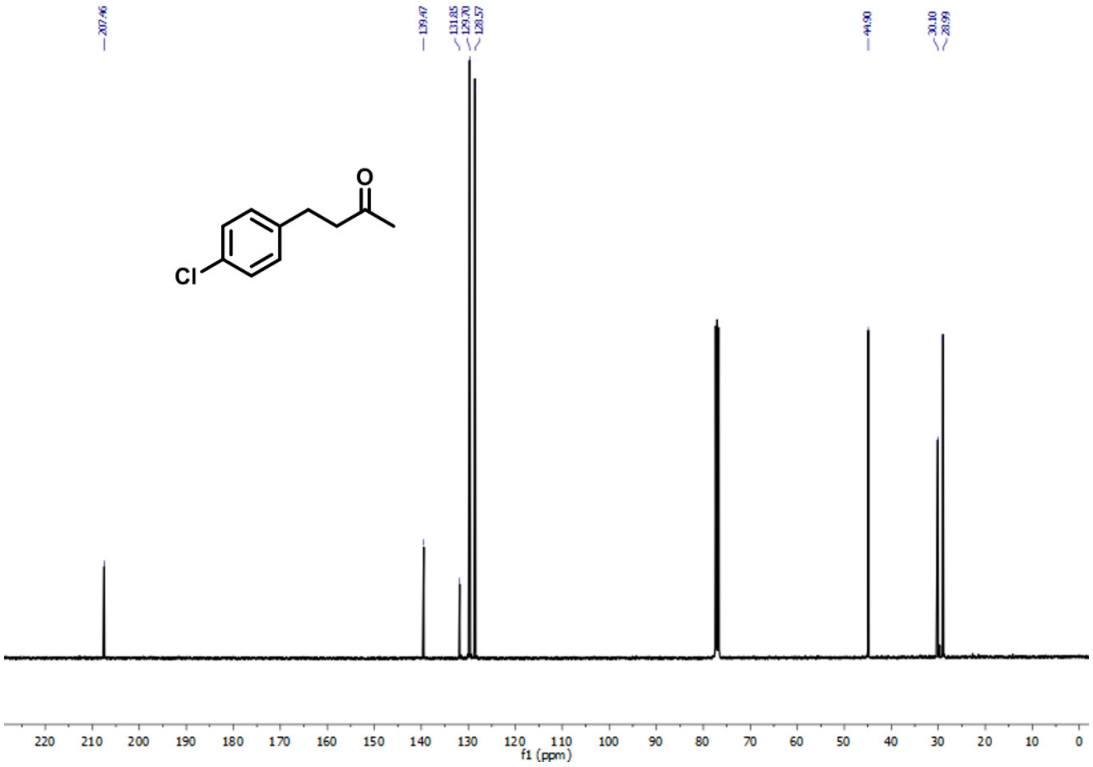

Figure S55. ^{13}C NMR spectrum of product **6d**.

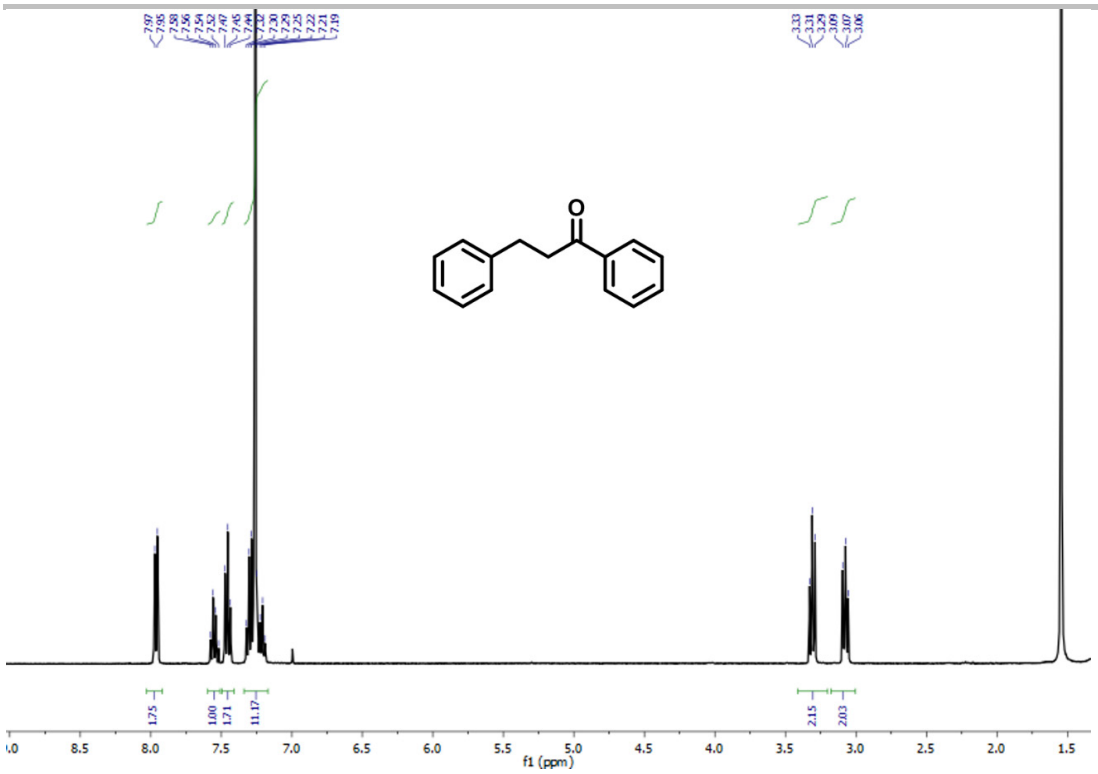

Figure S56. ^{1}H NMR spectrum of product **6e**.

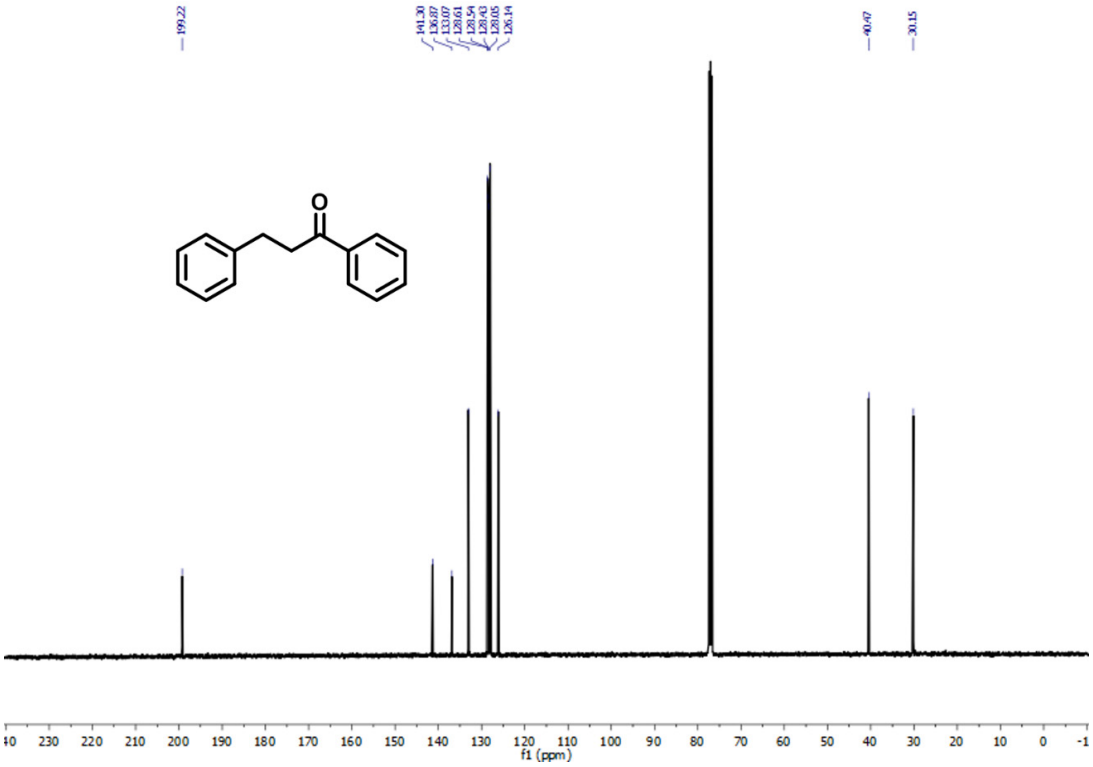

Figure S57. ^{13}C NMR spectrum of product **6e**.

Figure S58. ^{1}H NMR spectrum of product **6f**.

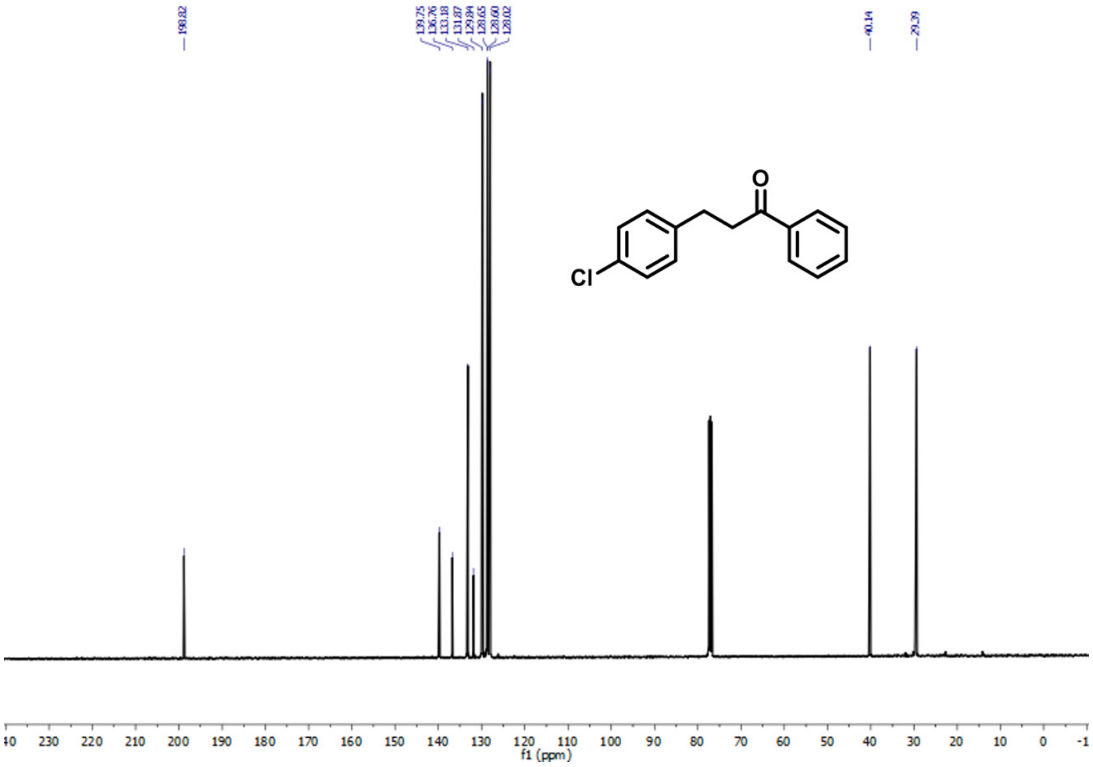

Figure S59. ^{13}C NMR spectrum of product **6f**.

8. References

[1] C. Q. Zhao, Y. G. Chen, H. Qiu, L. Wei, P. Fang, T. S. Mei, *Org. Lett.* **2019**, *21*, 1412-1416.

[2] E. D. Bloch, D. Britt, C. Lee, C. J. Doonan, F. J. Uribe-Romo, H. Furukawa, J. R. Long, O. M. Yaghi, *J. Am. Chem. Soc.* **2010**, *132*, 14382-14384.

[3] A. M. Hengne, A. K. Samal, L. R. Enakonda, M. Harb, L. E. Gevers, D. H. Anjum, M. N. Hedhili, Y. Saih, K. W. Huang, J. M. Basset, *ACS Omega* **2018**, *3*, 3688-3701.

[4] P. Ji, K. Manna, Z. Lin, A. Urban, F. X. Greene, G. Lan, W. Lin, *J. Am. Chem. Soc.* **2016**, *138*, 12234-12242.

[5] X. Feng, Y. Song, J. S. Chen, Z. Li, E. Y. Chen, M. Kaufmann, C. Wang, W. Lin, *Chem. Sci.* **2019**, *10*, 2193-2198.

[6] M. J. Frisch, G. W. Trucks, H. B. Schlegel, G. E. Scuseria, M. A. Robb, J. R. Cheeseman, G. Scalmani, V. Barone, G. A. Petersson, H. Nakatsuji, X. Li, M. Caricato, A. V. Marenich, J. Bloino, B. G. Janesko, R. Gomperts, B. Mennucci, H. P. Hratchian, J. V. Ortiz, A. F. Izmaylov, J. L. Sonnenberg, Williams, F. Ding, F. Lipparini, F. Egidi, J. Goings, B. Peng, A. Petrone, T. Henderson, D. Ranasinghe, V. G. Zakrzewski, J. Gao, N. Rega, G. Zheng, W. Liang, M. Hada, M. Ehara, K. Toyota, R. Fukuda, J. Hasegawa, M. Ishida, T. Nakajima, Y. Honda, O. Kitao, H. Nakai, T. Vreven, K. Throssell, J. A. Montgomery Jr., J. E. Peralta, F. Ogliaro, M. J. Bearpark, J. J. Heyd, E. N. Brothers, K. N. Kudin, V. N. Staroverov, T. A. Keith, R. Kobayashi, J. Normand, K. Raghavachari, A. P. Rendell, J. C. Burant, S. S. Iyengar, J. Tomasi, M. Cossi, J. M. Millam, M. Klene, C. Adamo, R. Cammi, J. W. Ochterski, R. L. Martin, K. Morokuma, O. Farkas, J. B. Foresman, D. J. Fox, Gaussian 16 Rev. C.01, Wallingford, CT, **2016**.

[7] A. D. Becke, *Phys. Rev. A* **1988**, *38*, 3098-3100.

[8] S. Grimme, S. Ehrlich, L. Goerigk, *J. Comput. Chem.* **2011**, *32*, 1456-1465.

[9] C. Lee, W. Yang, R. G. Parr, *Phys. Rev. B* **1988**, *37*, 785-789.

[10] I. Senkovska, F. Hoffmann, M. Fröba, J. Getzschmann, W. Böhlmann, S. Kaskel, *Microporous and Mesoporous Mater.* **2009**, *122*, 93-98.

[11] M. Gupta, E. F. da Silva, H. F. Svendsen, *J. Phys. Chem. B* **2016**, *120*, 9034-9050.

[12] A. V. Marenich, C. J. Cramer, D. G. Truhlar, *J. Phys. Chem. B* **2009**, *113*, 6378-6396.